NAVIGATION BASED PATH PLANNING

BY OPTIMAL CONTROL THEORY

A Thesis

Submitted to the Faculty

of

Purdue University

by

Sean Matthew Nolan

In Partial Fulfillment of the

Requirements for the Degree

of

Master of Science in Aeronautics and Astronautics

December 2018

Purdue University

West Lafayette, Indiana

THE PURDUE UNIVERSITY GRADUATE SCHOOL
STATEMENT OF THESIS APPROVAL

Dr. Michael J. Grant, Chair

School of Aeronautics and Astronautics

Dr. Adam J. Rutkowski

Air Force Research Laboratory

Dr. Inseok Hwang

School of Aeronautics and Astronautics

Approved by:

Dr. Wayne Chen

Aeronautics and Astronautics Associate Head for Graduate Education

To my loving family, my darling Mary, and the greater glory of God

"But man does not create...he discovers." – Antonio Gaudi

ACKNOWLEDGMENTS

Firstly, I thank my parents Jim and Suzana and my brother Jim who have always been there with ample love and support. Also, I want to thank my wonderful fiancée Mary who makes my work worth any difficulty. I am extraordinary grateful to my advisor Dr. Michael Grant who has gone above and beyond as an advisor. His guidance, motivation, and patience were indispensable to me not only for this work but also for my graduate school career. I am also thankful to Dr. Adam Rutkowski for his assistance to formulate and solve these problems. Without him, this thesis would not exist. I am also thankful for the Mathematical Modeling and Optimization Institute for allowing me to spend a summer dedicated to this research. I also thank Dr. Inseok Hwang for being on my committee and his instruction through his class. Dr. Daniel DeLaurentis deserves special acknowledgment for assisting me finish this work. Lastly, I greatly appreciate my fellow lab members for their previous work and assistance to me, especially Thomas Antony, Michael Sparapany, and Kshitij Mall whose work was vital to mine.

TABLE OF CONTENTS

Page

LIST OF FIGURES

SYMBOLS

A_{ref}	reference area
AR	aspect ratio
a	step length
C_D	drag coefficient
C_L	lift coefficient
D	drag
e_0	Oswald efficiency factor
F	linearization of dynamics w.r.t. states
$\boldsymbol{f}$	dynamics vector
G	continuous time transformation from process noise to states
g	acceleration due to gravity
$\bar{\boldsymbol{g}}$	residual function
H	linearization of measurements w.r.t. states
$\mathcal{H}$	Hamiltonian
$\boldsymbol{h}$	measurement vector
h	altitude
$\mathbb{I}$	identity matrix
J	cost/objective functional
$\mathbb{J}$	Jacobian
K	Kalman filter gain
K_{cov}	covariance scaling matrix
k_{en}	control energy scaling constant
k_{cov}	covariance scaling constant
k_{norm}	norm scaling constant
L	lift

$\mathcal{L}$	path cost integrand
m	mass
P	covariance matrix
$\bar{\boldsymbol{p}}$	parameter vector
p	covariance matrix element
Q	state process noise covariance matrix
R	measurement noise covariance matrix
s	aircraft descent downrange
t	time
$\boldsymbol{u}$	control vector
$\boldsymbol{v}$	measurement noise
v	velocity
$\boldsymbol{w}$	state process noise
$\boldsymbol{x}$	state vector
x	cart problem downrange
$\boldsymbol{y}$	measurement
y	cart problem crossrange
α	angle of attack
β	bearing angle
$\boldsymbol{\epsilon}$	shooting method residual
ϵ	constant for smoothing term
θ	heading angle
$\boldsymbol{\lambda}$	costate vector
ν	Lagrange multiplier
ρ	range measurement
ϱ	density
σ	standard deviation
Υ	discrete time transformation from process noise to states
Φ	terminal cost with adjoined terminal constraints

$\boldsymbol{\Phi}$	state-transition matrix
ϕ	terminal cost
$\boldsymbol{\Psi}$	boundary condition vector
ω	turn rate

ABBREVIATIONS

BVP	boundary value problem
DAE	differential-algebraic system of equations
EFK	extended Kalman filter
EOM	equations of motion
GTSAM	Georgia Tech Smoothing and Mapping
MSM	multiple shooting method
OCT	optimal control theory
SSM	single shooting method
STM	state-transition matrix
TPBVP	two-point boundary value problem

ABSTRACT

Nolan, Sean M. M.S.A.A., Purdue University, December 2018. Navigation Based Path Planning by Optimal Control Theory. Major Professor: Michael J. Grant.

Previous studies have shown that implementing trajectory optimization can reduce state estimations errors. These navigation based path planning problems are often difficult to solve being computationally burdensome and exhibiting other numerical issues, so former studies have often used lower-fidelity methods or lacked explanatory power.

This work utilizes indirect optimization methods, particularly optimal control theory, to obtain high-quality solutions minimizing state estimation errors approximated by a continuous-time extended Kalman filter. Indirect methods are well-suited to this because necessary conditions of optimality are found prior to discretization and numerical computation. They are also highly parallelizable enabling application to increasingly larger problems.

A simple one dimensional problem shows some potential obstacles to solving problems of this type including regions of the trajectory where the control is unimportant. Indirect trajectory optimization is applied to a more complex scenario to minimize location estimation errors of a single cart traveling in a 2-D plane to a goal location and measuring range from a fixed beacon. This resulted in a 96% reduction of the location error variance when compared to the minimum time solution. The single cart problem also highlights the importance of the matrix that encodes the linearization of the vehicle's measurement with respect to state. It is shown in this case that the vehicle roughly attempts to maximize the magnitude of its elements. Additionally, the cart problem further illustrates problematic regions of a design space where the objective is not significantly affected by the trajectory.

An aircraft descent problem demonstrates the applicability of these methods to aerospace problems. In this case, estimation error variance is reduced 28.6% relative to the maximum terminal energy trajectory. Results are shown from two formulations of this problem, one with control constraints and one with control energy cost, to show the benefits and disadvantages of the two methods. Furthermore, the ability to perform trade studies on vehicle and trajectory parameters is shown with this problem by solving for different terminal velocities and different initial locations.

1. INTRODUCTION AND MOTIVATION

The traditional mission planning process contains two distinct and separate phases. One is the design of a nominal reference trajectory, which is considered to be deterministic. The other is navigation guidance that commands changes to the control to minimize deviations from the reference amid uncertainties during the mission. By separating these two phases, the designer may miss an opportunity to reduce state estimation errors through changing the vehicle's path. Several previous studies have already shown that changing a vehicle's path can reduce the size of state estimation errors significantly. Unfortunately, many of these studies lack explanatory power because they only survey a limited space of trajectories.

As early as 1968, a paper demonstrates that ability and outlines a process using optimal control theory like in this thesis to minimize estimation errors in a trajectory [1]. D. R. Vander Stoep applied the process only to a one dimensional problem with linear control and bearing angle measurement similar to the problem in Section 4.2. The application of the process at the time would be limited by the computational capability at the time.

Other more recent research has investigated the use of trajectories to minimize state errors. These studies have largely only used zeroth-order optimization methods. These zeroth-order methods, which do not use derivatives to find the optimal solution, are relatively easy to implement and can be applied to fairly complex problems, but they also have significant disadvantages. Important information provided by the derivatives is lost, and truly optimal solutions are not guaranteed unless all possible paths are evaluated. This results in the restriction of the solutions to a finite set, which often leads to low fidelity solutions, and the search through the entire set can be rather computationally intensive. If the form of the control law is defined a priori, better solutions cannot be reached, and the process excludes equally feasible

trajectories that elucidate the characteristics that fundamentally lead to a better result.

Bryson and Sukkarieh have an UAV reduce estimation error by occasionally executing either s-shape or orbit maneuvers to increase observability of states [2]. Bose and Richards investigates optimal paths for the most accurate simultaneous location and mapping (SLAM) using Sequential Monte Carlo optimization, which is similar to a particle filter [3]. Rutkowski showed by maneuvering vehicles with measurements from an IMU and vision system in a "zig-zagging" curved trajectory can more accurately perform SLAM when compared to a straight path and that the frequency and magnitude of the curves affect the error reduction [4].

Rutkowski with others also investigated cooperative navigation between two carts with a range measurement between them [5, 6]. This problem is shown with detail in Section 4.1 as a motivating problem. The first study searched for the most accurate trajectory among candidate trajectories formed by placing 10 different waypoints either to the left or right to the previous one. Because one cart can follow $\frac{10!}{(5!)^2} = 252$ possible paths, there are 63,504 combinations to study. This method resulted in reducing the standard deviation by a factor of 5 compared to the case where the carts traveled directly toward the goal [5]. The second study expands upon the first using a random search algorithm. Several waypoints were placed by randomly perturbing the currently best performing set of waypoints. If the new waypoints performed better, future trials were perturbed from it. This method yielded a nearly 15 factor reduction in position uncertainty standard deviation [6].

There is research that does use higher order optimization techniques, but the studies required concessions to make the problems tractable. Watanabe uses a "one-step-ahead" suboptimal optimization technique that solves an approximate problem for the next time step [7]. Small uses direct optimization methods to solve navigation based problems, but problem size requires covariance values to be calculated separately from the interpolated states and no attempt is made to provide an explanatory hypothesis of why the results follow the path they do [8].

The goal of the work presented here is to use indirect optimization to obtain high-quality solutions to these navigation based path planning problems. By doing so, a designer can gain greater insight into what characteristics in a vehicle's path lead to better error estimation. Indirect methods and the implementation explained in Section 2.1 are well-suited to obtaining high-quality solutions because necessary conditions of optimality are derived prior to discretization needed to numerically arrive at a solution. Indirect methods also have the benefits of not exhibiting numerical artifacts like control jitters present from direct methods, having better computational scaling than direct methods, and being highly parallelizable [9].

Having the ability to form these optimal solutions enables researchers to analyze these optimal trajectories for traits that may be applied more generally and to perform trade studies to balance navigation considerations with other performance metrics. Furthermore, lessons learned in this work are especially helpful in solving more complex navigation based optimization problems in the future such as the dual-cart problem as well as other large trajectory optimization problems. Particularly, analyses of a single vehicle variant of the mentioned dual-cart problem and a gliding descent problem for a projectile demonstrate the utility of indirect methods for solving minimum estimation error trajectory problems.

2. OVERVIEW OF UNDERLYING THEORY AND TOOLS

This chapter reviews the theory that forms the foundation needed to minimize estimation errors using indirect trajectory optimization. Naturally, the two required areas are the optimization method (i.e. optimal control theory) and the state estimation method (accomplished with an extended Kalman filter).

2.1 Optimal Control Theory

There exists two branches of optimization. The first being the more common parameter optimization, which minimizes a function of a finite number of discrete variables and has its basis in calculus [10]. The other branch, optimal control theory (OCT), seeks to find solutions to problems of infinite dimension that minimize functionals and is based more specifically in calculus of variations [10]. This distinction is related to the distinction between direct and indirect methods in trajectory optimization. Direct methods, typically using parameter optimization, first discretize a problem's state and control variables and then adjusts them directly to minimize the objective function. Indirect methods instead start by applying optimal control to find the optimality conditions in terms of adjoint differential equations, minimum principle, and boundary conditions. These are used in most cases to solve a multi-point boundary value problem (BVP) using a root-solving algorithm [11]. According to [11], direct methods have been preferred to indirect methods in the recent decades because:

1. "It is necessary to derive analytic expressions for the necessary conditions, and for complicated nonlinear dynamics this can become quite daunting."

2. "The region of convergence for a root-finding algorithm may be surprisingly small, especially when it is necessary to guess values for the adjoint variables that may not have an obvious physical interpretation."

3. "For problems with path inequalities it is necessary to guess the sequence of constrained and unconstrained subarcs before iteration can begin."

These deficiencies have been largely addressed by previous work. Using symbolic computer algebra systems mitigates the requirement to derive necessary conditions manually, and the small region of convergence can be avoided by using a homotopy continuation strategy [12]. There are several ways to bypass the need for multiple arcs when dealing with path constraints. As the scope of this report only includes path constraints on the control, the work from [13] will be used as shown in Section 3.4.1. With those concerns addressed, indirect methods were chosen for the work presented here because they provide high quality solutions. Furthermore, through parallelization, they have the ability to computationally scale better than direct method solvers to handle these large problems [9].

Both obtaining higher quality solutions and solving more complex or longer trajectories require more discretization nodes when using direct methods. Because sensitivity information is calculated at each node, the addition of nodes contribute significantly to the curse of dimensionality at a quicker rate than indirect methods. The quality of solution also suffers with direct methods because numerical artifacts may appear such as high-frequency jitters as are often seen with highly sensitive problems. The solver directly manipulates the control variables to satisfies constraints and dynamics, and a control profile that changes rapidly, may be able to satisfy these within tolerances. Another issue arises from the way nodes are placed in the common pseudo-spectral method like the state-of-the-art GPOPS-II [14]. With a pseudo-spectral method, nodes are grouped near the beginning and end of a trajectory where the dynamics and controls tend to be the least interesting. Ultimately, the most fun-

damental short-coming of direct methods are that they do not guarantee optimality of the solution because discretization is performed prior to optimization [15].

2.1.1 Necessary Conditions

The generalized statement of an optimal control problem is given in Eqs. (2.1) to (2.4) with time t, state vector $\boldsymbol{x}(t)$, and control vector $\boldsymbol{u}(t)$. The objective function is defined in Eq. (2.1) by adding the terminal cost ϕ to the functional that defines the path cost $\int_{t_0}^{t_f} \mathcal{L}\, dt$. The dynamics (Eq. (2.2)) for the system are held along each point of the trajectory. Initial constraint and terminal constraint functions are defined by Eq. (2.3) and Eq. (2.4), respectively. The initial time, t_0, will be considered fixed, but final time t_f is free. Additional constraints can be added such as path, control, and interior point constraints as describe in [16], but for this work, the control constraints were applied by restructuring the problem using the method in [13], and path and interior point constraints were not required.

$$\min J = \phi[t_f, \boldsymbol{x}(t_f)] + \int_{t_0}^{t_f} \mathcal{L}[t, \boldsymbol{x}(t), \boldsymbol{u}(t)]\, dt \tag{2.1}$$

Subject to:

$$\dot{\boldsymbol{x}} = \boldsymbol{f}[t, \boldsymbol{x}(t), \boldsymbol{u}(t)] \tag{2.2}$$

$$0 = \boldsymbol{\Psi}_0[\boldsymbol{x}(t_0), t_0] \tag{2.3}$$

$$0 = \boldsymbol{\Psi}_f[\boldsymbol{x}(t_f), t_f] \tag{2.4}$$

To enforce the constraints above, they are adjoined to J using Lagrange Multipliers in Eq. (2.5). The dynamics constraint $(\boldsymbol{f} - \dot{\boldsymbol{x}})$ is applied with multiplier functions $\boldsymbol{\lambda}$ to the path cost. Note that the Lagrange multipliers $\boldsymbol{\lambda}$ are referred to as costates and vary with time. The initial and terminal constraints are adjoined to the terminal cost with constant multipliers $\boldsymbol{\nu}_0$ and $\boldsymbol{\nu}_f$.

$$\begin{aligned}\bar{J} &= \phi[t_f, \boldsymbol{x}(t_f)] + \boldsymbol{\nu}_0^T \boldsymbol{\Psi}_0[\boldsymbol{x}(t_0), t_0] + \boldsymbol{\nu}_f^T \boldsymbol{\Psi}_f[\boldsymbol{x}(t_f), t_f] \\ &+ \int_{t_0}^{t_f} \mathcal{L}[t, \boldsymbol{x}(t), \boldsymbol{u}(t)] + \boldsymbol{\lambda}^T(t)(\boldsymbol{f}[t, \boldsymbol{x}(t), \boldsymbol{u}(t)] - \dot{\boldsymbol{x}})\, dt\end{aligned} \tag{2.5}$$

It is convenient to define the scalar function $\mathcal{H} = \mathcal{L} + \boldsymbol{\lambda}^T \boldsymbol{f}$ referred to as the Hamiltonian. Also, terminal constraints are combined with the terminal cost $\Phi = \phi + \boldsymbol{\nu}_f^T \boldsymbol{\Psi}_f$. This gives Eq. (2.6). The function arguments are dropped for conciseness.

$$\bar{J} = \Phi + \boldsymbol{\nu}_0^T \boldsymbol{\Psi}_0 + \int_{t_0}^{t_f} (\mathcal{H} - \boldsymbol{\lambda}^T \dot{\boldsymbol{x}})\, dt \tag{2.6}$$

A necessary condition of optimality is that the differential of $\bar{J}$ must equal 0. Equation (2.7) shows the differential of $\bar{J}$ with respect to differential changes in $\boldsymbol{x}$ and t_f.

$$\begin{aligned}d\bar{J} &= \left[\left(\frac{\partial \Phi}{\partial t} + \mathcal{L}\right) dt + \frac{\partial \Phi}{\partial \boldsymbol{x}} d\boldsymbol{x}\right]_{t=t_f} + \left[\left(\boldsymbol{\nu}_0 \frac{\partial \Psi_0}{\partial t} - \mathcal{L}\right) dt + \boldsymbol{\nu}_0 \frac{\partial \Psi_0}{\partial \boldsymbol{x}} d\boldsymbol{x}\right]_{t=t_0} \\ &+ \int_{t_0}^{t_f} \left(\frac{\partial \mathcal{H}}{\partial \boldsymbol{x}} \delta \boldsymbol{x} + \frac{\partial \mathcal{H}}{\partial u} \delta u - \boldsymbol{\lambda}^T \delta \dot{\boldsymbol{x}}\right) dt = 0\end{aligned} \tag{2.7}$$

By integrating by parts, using $\delta \boldsymbol{x} = d\boldsymbol{x} - \dot{\boldsymbol{x}} dt$, and noting $dt|_{t=t_0} = 0$, Eq. (2.8) is obtained.

$$\begin{aligned}d\bar{J} &= \left(\frac{\partial \Phi}{\partial t} + \mathcal{L} + \boldsymbol{\lambda}^T \dot{\boldsymbol{x}}\right)_{t=t_f} dt_f + \left[\left(\frac{\partial \Phi}{\partial \boldsymbol{x}} - \boldsymbol{\lambda}^T\right) d\boldsymbol{x}\right]_{t=t_f} \\ &+ \left[\left(\boldsymbol{\nu}_0 \frac{\partial \Psi_0}{\partial \boldsymbol{x}} + \boldsymbol{\lambda}^T\right) d\boldsymbol{x}\right]_{t=t_0} + \int_{t_0}^{t_f} \left[\left(\frac{\partial \mathcal{H}}{\partial \boldsymbol{x}} + \dot{\boldsymbol{\lambda}}\right) \delta \boldsymbol{x} + \frac{\partial \mathcal{H}}{\partial u} \delta u\right] dt = 0\end{aligned} \tag{2.8}$$

The final expressions for necessary conditions are obtained finally in Eqs. (2.9) to (2.13) by equating each term in Eq. (2.8) to 0.

$$\dot{\boldsymbol{\lambda}} = -\frac{\partial \mathcal{H}}{\partial \boldsymbol{x}} \tag{2.9}$$

$$\boldsymbol{\lambda}(t_0) = \left(-\boldsymbol{\nu}_0^T \frac{\partial \Psi_0}{\partial \boldsymbol{x}}\right)_{t=t_0} \tag{2.10}$$

$$\boldsymbol{\lambda}(t_f) = \left(\frac{\partial \Phi}{\partial \boldsymbol{x}}\right)_{t=t_f} = \left(\frac{\partial \phi}{\partial \boldsymbol{x}} + \boldsymbol{\nu}_f^T \frac{\partial \Psi_f}{\partial \boldsymbol{x}}\right)_{t=t_f} \tag{2.11}$$

$$\begin{aligned} 0 &= \left(\frac{\partial \Phi}{\partial t} + \mathcal{L} + \boldsymbol{\lambda}^T \dot{\boldsymbol{x}}\right)_{t=t_f} \\ &= \left(\frac{\partial \Phi}{\partial t} + \frac{\partial \Phi}{\partial \boldsymbol{x}} \dot{\boldsymbol{x}} + \mathcal{L}\right)_{t=t_f} \\ &= \left(\frac{d\Phi}{dt} + \mathcal{L}\right)_{t=t_f} \end{aligned} \tag{2.12}$$

$$\frac{\partial \mathcal{H}}{\partial u} = 0 \tag{2.13}$$

The problem is now expressible as a two-point boundary value problem (TPBVP). Equation (2.9) defines the dynamics for the costates. Equation (2.10), Eq. (2.11), and Eq. (2.12) provide the needed boundary conditions (BCs). Equation (2.13) gives an algebraic expression for the control law. If that expression is not sufficient, the Pontryagrin minimum principle must be used shown in Eq. (2.14).

$$\mathcal{H}\left[t, \boldsymbol{x}^*(t), \boldsymbol{u}^*(t), \boldsymbol{\lambda}^*(t),\right] \leq \mathcal{H}\left[t, \boldsymbol{x}^*(t), \boldsymbol{u}, \boldsymbol{\lambda}^*(t),\right] \tag{2.14}$$

2.1.2 Description of Solver Implementation

It is helpful for the work done here to have a brief description of the solver's implementation of the OCT. The solver, named Beluga, is a product from Michael Grant's lab. A flowchart that summarizes the solution process is given in Fig. 2.1. In order to overcome the small radius of convergence of the indirect method, Beluga uses a homotopic continuation process following [12]. This continuation process starts by solving a relatively small problem using an initial guess formed by propagating the trajectory with guesses for the unknown states, costates, and parameters. The

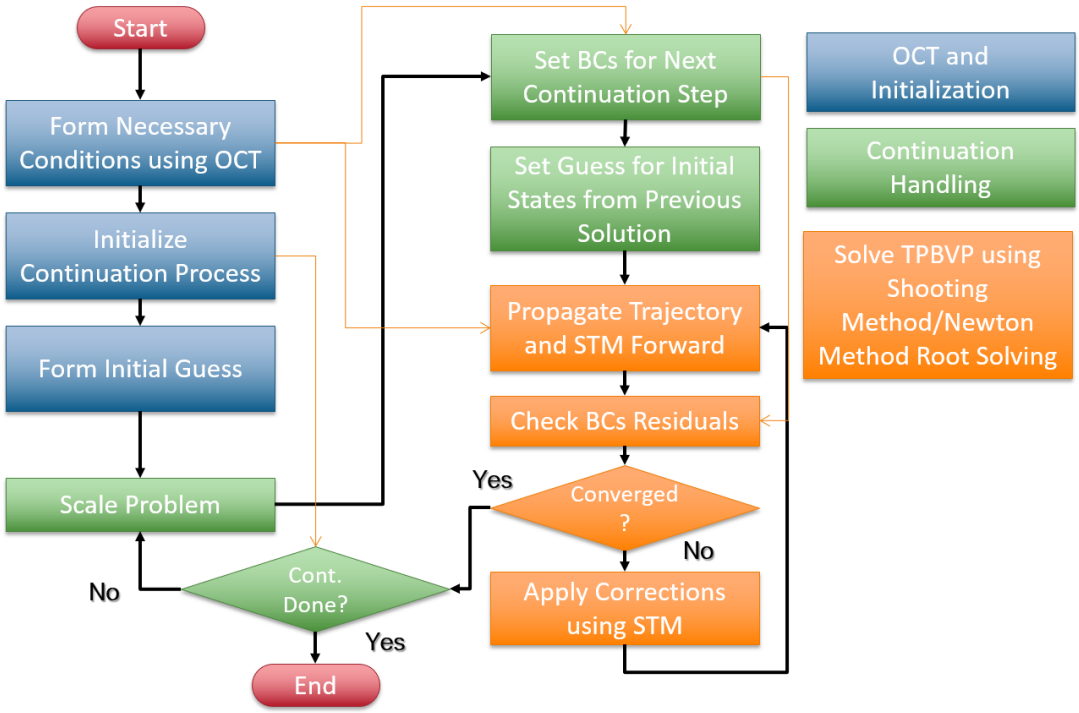

Figure 2.1. Flowchart of Trajectory Optimization Process (Beluga)

solution to that small problem is then used as an initial guess to a "larger" problem with boundary conditions and any other parameters closer to the final problem of interest. This new solution problem is used again as an initial guess to an even "larger" problem. The process is repeated until the desired BC and parameters are reached. An example of this continuation process applied to a navigation problem is shown in Fig. 2.2.

For the work presented here, the TPBVP posed by applying OCT is solved using the Multiple Shooting Method (MSM). This method is built upon the Single Shooting Method (SSM). With SSM, the equations of motion (EOM) are integrated from the guesses for the free initial states, costates, and parameters. The terminal boundary conditions are evaluated to obtain a residual error vector as in Eq. (2.15)

$$\bar{\boldsymbol{g}}\left(\boldsymbol{x}_0, \boldsymbol{x}_f, \boldsymbol{\lambda}_0, \boldsymbol{\lambda}_f, \bar{\boldsymbol{p}}\right) = \boldsymbol{\varepsilon} \tag{2.15}$$

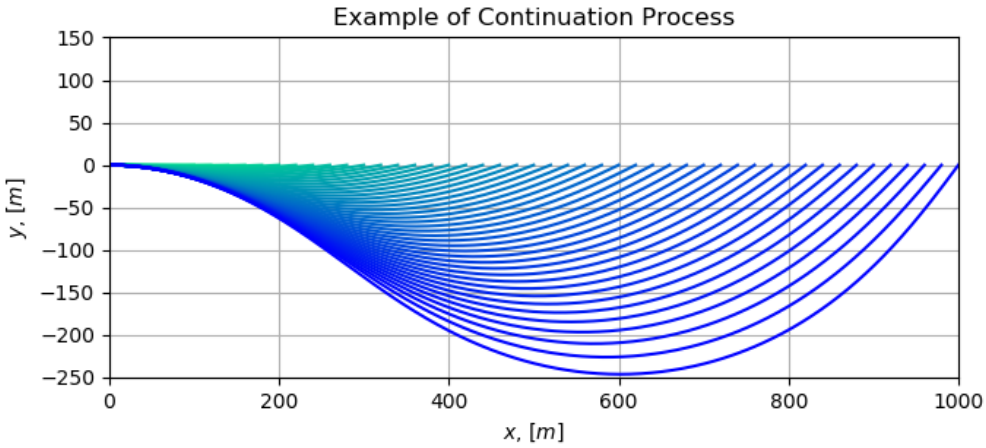

Figure 2.2. Example of Continuation Applied to Navigation Problem in Section 4.3

Corrections need to be made to drive the residual error to zero. A first-order approximation for the correction is formulated using the Jacobian matrices in Eq. (2.16) and state-transition matrix (STM) defined in Eq. (2.17) propagated along with the EOMs. Corrections to free parameters require $\frac{d\boldsymbol{x}_f}{d\bar{\boldsymbol{p}}}$ calculated in nearly the same way as the STM. These form a combined Jacobian Eq. (2.18), which is used to form the modified Newton's step in Eq. (2.19) to be applied to the initial guess where a is a specified step-length. The correction is applied, and the process is repeated until the residual becomes sufficiently small.

$$\mathbb{J}_M = \frac{\partial \bar{g}}{\partial \boldsymbol{x}_0}, \quad \mathbb{J}_N = \frac{\partial \bar{g}}{\partial \boldsymbol{x}_f}, \quad \mathbb{J}_P = \frac{\partial \bar{g}}{\partial \bar{\boldsymbol{p}}} \tag{2.16}$$

$$\Phi = \frac{d\boldsymbol{x}\left(t\right)}{d\boldsymbol{x}_0}, \quad \dot{\Phi} = \frac{\partial \boldsymbol{f}}{\partial \boldsymbol{x}}\Phi, \quad \Phi\left(t_0\right) = \mathbb{I} \tag{2.17}$$

$$\mathbb{J} = \begin{bmatrix} \mathbb{J}_M + \mathbb{J}_N\Phi & \mathbb{J}_P + \mathbb{J}_N\frac{d\boldsymbol{x}_f}{d\bar{\boldsymbol{p}}} \end{bmatrix} \tag{2.18}$$

$$\begin{bmatrix} \Delta\boldsymbol{x}_0 \\ \Delta\bar{\boldsymbol{p}} \end{bmatrix} = -a\mathbb{J}^{-1}\boldsymbol{\varepsilon} \tag{2.19}$$

Multiple Shooting varies from SSM in that it divides the trajectory into multiple arcs that are propagated separately. The original initial conditions hold as well as the condition that the trajectory must be continuous between arcs as seen in Eq. (2.20). Likewise, Jacobians are defined by Eq. (2.21) for the beginning and end of each arc, and the system Jacobian is given by Eq. (2.22).

$$\bar{\boldsymbol{g}}\left(\boldsymbol{x}_0, \boldsymbol{x}_f, \bar{p}\right) = \Psi_0\left(\boldsymbol{x}_0\right) + \Psi_f\left(\boldsymbol{x}_f\right) + \sum_{i=2}^{n}\left(\boldsymbol{x}\left(t_i^+\right) - \boldsymbol{x}\left(t_{i-1}^-\right)\right) \tag{2.20}$$

$$\mathbb{J}_{M_i} = \frac{\partial \bar{g}}{\partial \boldsymbol{x}\left(t_i^+\right)}, \; \mathbb{J}_{N_i} = \frac{\partial \bar{g}}{\partial \boldsymbol{x}\left(t_i^-\right)}, \; \mathbb{J}_P = \frac{\partial \bar{g}}{\partial \bar{\boldsymbol{p}}} \tag{2.21}$$

$$\mathbb{J} = \begin{bmatrix} \mathbb{J}_{M_1} + \mathbb{J}_{N_1}\Phi_1 & \mathbb{J}_{M_2} + \mathbb{J}_{N_2}\Phi_2 & \cdots & \mathbb{J}_{M_n} + \mathbb{J}_{N_n}\Phi_n & \mathbb{J}_P + \sum_{i=1}^{n}\mathbb{J}_{N_i}\frac{d\boldsymbol{x}\left(t_i^-\right)}{d\bar{\boldsymbol{p}}} \end{bmatrix} \tag{2.22}$$

With the new Jacobian, the problem can be solved using the same step as SSM.

Because each arc is significantly shorter than originally, MSM reduces numerical issues that arise if a problem has EOMs that are very sensitive to initial conditions. Through experience, this has shown necessary for these navigation based problems.

Furthermore, each arc can be propagated in parallel reducing computation time as discussed in Section 3.2.1.

2.2 State Estimation

The other significant portion of the navigation based problem is the estimation of states and particularly quantifying the expected size of the estimation errors. This will require calculating the covariance matrix P in which the diagonal elements are the squares of each state's error standard deviation, σ_i^2, and the off diagonal elements are the two states' standard deviations multiplied by the two states' correlation coefficient, $\rho_{i,j}\sigma_i\sigma_j$. The objective of navigation based path planning is to minimize one or a combination of the diagonal variance elements by modifying the path. A state estimator, as the name implies, synthesizes stochastic information about the vehicle's dynamics and measurements to estimate the vehicle's states. They usually produce the covariance matrix that is needed. In this work, state estimators are only of concern to give an estimate of P and their direct improvement will not be considered.

2.2.1 First Order Filter Example

To gain some fundamental understanding of state estimation, the following simple first-order filter example is helpful [17]. The simple system has the "truth" modeled by Eq. (2.23).

$$\begin{aligned} \dot{x}(t) &= Fx(t),\ x(t_0) = 1 \\ \tilde{y}(t) &= Hx(t) + v(t) \\ F &= -1,\ H = 1 \end{aligned} \tag{2.23}$$

Assuming that $v(t)$ is zero mean Gaussian noise with standard deviation 0.05, this process is simulated in Fig. 2.3. Suppose that value for F is not known, and the measurement must be used to estimate the state x. The linear feedback system in

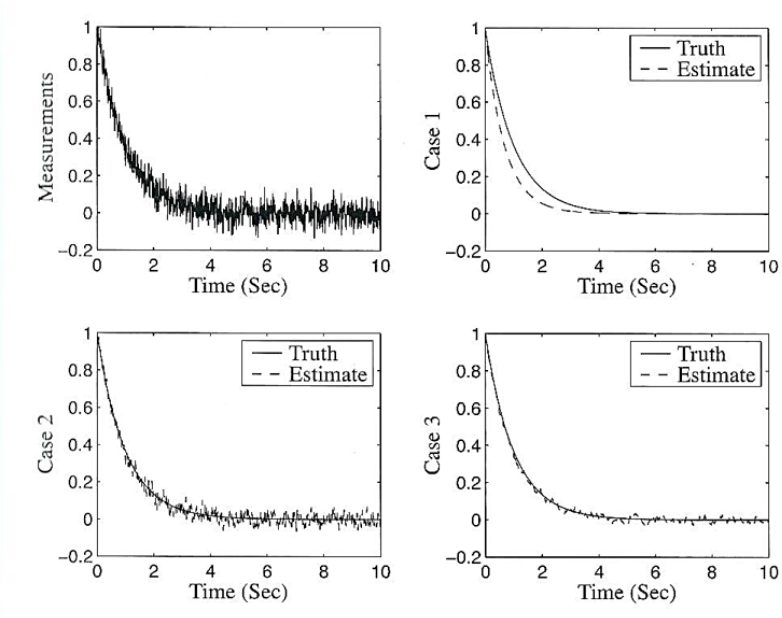

Figure 2.3. First-Order Filter Example [17]

Eq. (2.24) to drive the estimated state $\hat{x}$ to x by feeding back the difference between actual measurement and the expected measurement $\hat{y}$.

$$\begin{aligned} \dot{\hat{x}}(t) &= \bar{F}\hat{x}(t) + K\left[\tilde{y}(t) - H\hat{x}(t)\right] \\ \hat{y}(t) &= H\hat{x}(t) \end{aligned} \tag{2.24}$$

Figure 2.3 shows the result of the estimation for $\bar{F} = -1.5$ and K values of 0.1, 100, and 15 for Case 1, Case 2, and Case 3 respectively. As can be seen, the estimate in Case 1 is affected little by the measurement. This results in an estimate that is smooth because it uses mainly the model, but it cannot correct for the error in the model and varies significantly from the true value. Case 2 relies heavily on the measurement, so it closely follows the truth value, yet the estimate is greatly affected by the measurement causing relatively large fluctuations. Case 3 appears to be the best of the three presented. The estimate follows the truth from the corrections from the measurement, and the dynamic model adequately smooths fluctuations from the noise.

2.2.2 Continuous-Time Kalman Filter

This section concerns finding the optimal gain for an estimator of a linear system. This optimal estimator is referred to as the Kalman filter. The continuous version is derived here because the continuous formulation is most conducive to integrating with OCT. The truth model is given in Eq. (2.25) with states $\boldsymbol{x}(t)$, controls $\boldsymbol{u}(t)$ and measurements $\tilde{\boldsymbol{y}}(t)$.

$$\begin{aligned} \dot{\boldsymbol{x}}(t) &= F(t)\boldsymbol{x}(t) + B(t)\boldsymbol{u}(t) + G(t)\boldsymbol{w}(t) \\ \tilde{\boldsymbol{y}}(t) &= H(t)\boldsymbol{x}(t) + \boldsymbol{v}(t) \end{aligned} \tag{2.25}$$

The stochastic variables $\boldsymbol{w}(t)$ and $\boldsymbol{v}(t)$ are zero-mean Gaussian noise processes with covariances given by Eq. (2.26).

$$\begin{aligned} E\left\{\boldsymbol{w}(t)\boldsymbol{w}^T(\tau)\right\} &= Q(t)\delta\left(t-\tau\right) \\ E\left\{\boldsymbol{v}(t)\boldsymbol{v}^T(\tau)\right\} &= R(t)\delta\left(t-\tau\right) \\ E\left\{\boldsymbol{v}(t)\boldsymbol{w}^T(\tau)\right\} &= 0 \end{aligned} \tag{2.26}$$

The Kalman filter's structure is prescribed as the feedback form given in Eq. (2.27).

$$\begin{aligned} \dot{\hat{\boldsymbol{x}}}(t) &= F(t)\hat{\boldsymbol{x}}(t) + B(t)\boldsymbol{u}(t) + K(t)\left[\tilde{\boldsymbol{y}}(t) - H(t)\hat{\boldsymbol{x}}\right] \\ \hat{\boldsymbol{y}}(t) &= H(t)\hat{\boldsymbol{x}}(t) \end{aligned} \tag{2.27}$$

The state error $\tilde{\boldsymbol{x}} = \hat{\boldsymbol{x}}(t) - \boldsymbol{x}(t)$ has dynamics described by Eq. (2.28).

$$\dot{\tilde{x}}(t) = E(t)\tilde{\boldsymbol{x}}(t) + \boldsymbol{z}(t) \tag{2.28}$$

where:

$$E(t) = F(t) - K(t)H(t) \tag{2.29}$$

$$\boldsymbol{z}(t) = -G(t)\boldsymbol{w}(t) + K(t)\boldsymbol{v}(t) \tag{2.30}$$

The covariance matrix for $\boldsymbol{z}$ is shown in Eq. (2.31) noting that $\boldsymbol{u}(t)$ cancels in the state error and that $\boldsymbol{v}(t)$ and $\boldsymbol{w}(t)$ are uncorrelated.

$$E\left\{\boldsymbol{z}(t)\boldsymbol{z}^T(\tau)\right\} = \left[G(t)Q(t)G(t)^T(t) + K(t)R(t)K^T(t)\right]\delta(t-\tau) \tag{2.31}$$

The matrix exponential solution of Eq. (2.32) is used to find the state error covariance $P(t)$ in Eq. (2.33).

$$\tilde{\boldsymbol{x}}(t) = \Phi(t, t_0)\tilde{\boldsymbol{x}}(t_0) + \int_{t_0}^{t} \Phi(t, \tau)\boldsymbol{z}(\tau)d\tau \tag{2.32}$$

$$\begin{aligned} P(t) &\equiv E\left\{\tilde{\boldsymbol{x}}(t)\tilde{\boldsymbol{x}}^T(t)\right\} \\ &= \Phi(t, t_0)P(t_0)\Phi^T(t, t_0) \\ &+ \int_{t_0}^{t} \Phi(t, \tau)\left[G(\tau)Q(\tau)G^T(\tau) + K(\tau)R(\tau)K^T(\tau)\right]\Phi^T(t, \tau)d\tau \end{aligned} \tag{2.33}$$

The time derivative of $P(t)$ is taken in Eq. (2.34).

$$\begin{aligned} \dot{P}(t) = &\frac{\partial\Phi(t, t_0)}{\partial t}P(t_0)\Phi^T(t, t_0) + \Phi(t, t_0)P(t_0)\frac{\partial\Phi^T(t, t_0)}{\partial t} \\ &+ \int_{t_0}^{t} \frac{\partial\Phi(t, \tau)}{\partial t}\left[G(\tau)Q(\tau)G^T(\tau) + K(\tau)R(\tau)K^T(\tau)\right]\Phi^T(t, \tau)d\tau \\ &+ \int_{t_0}^{t} \Phi(t, \tau)\left[G(\tau)Q(\tau)G^T(\tau) + K(\tau)R(\tau)K^T(\tau)\right]\frac{\partial\Phi^T(t, \tau)}{\partial t}d\tau \\ &+ \Phi(t, t)\left[G(t)Q(t)G^T(t) + K(t)R(t)K^T(t)\right]\Phi^T(t, t) \end{aligned} \tag{2.34}$$

Using several matrix exponential properties and Eqs. (2.29) and (2.33) simplify Eq. (2.34) to Eq. (2.35).

$$\begin{aligned} \dot{P}(t) = &\left[F(t) - K(t)H(t)\right]P(t) + P(t)\left[F(t) - K(t)H(t)\right]^T \\ &+ G(t)Q(t)G^T(t) + K(t)R(t)K^T(t) \end{aligned} \tag{2.35}$$

The gain $K(t)$ is now found to minimize the size of the diagonal elements (the state variances) of $P(t)$. This is accomplished by the equivalent problem of minimizing the trace of the time derivative $\dot{P}$.

$$\min J[K(t)] = \mathrm{Tr}[\dot{P}(t)] \tag{2.36}$$

This leads to holding the necessary condition Eq. (2.37), which is solved to give Eq. (2.38).

$$\frac{\partial J}{\partial K(t)} = 0 = 2K(t)R(t) - 2P(t)H^T(t) \tag{2.37}$$

$$K(t) = P(t)H^T(t)R^{-1}(t) \tag{2.38}$$

Substituting Eq. (2.38) in Eq. (2.33) gives the final expression for $\dot{P}(t)$ in Eq. (2.35).

$$\begin{aligned}\dot{P}(t) &= F(t)P(t) + P(t)F^T(t) \\ &\quad - P(t)H^T(t)R^{-1}(t)H(t)P(t) + G(t)Q(t)G^T(t)\end{aligned} \tag{2.39}$$

Another way to derive the continuous Kalman filter is from the discrete Kalman filter. This method is presented in [17]. That derivation provides relationships between the continuous $R(t)$ and $Q(t)$ and their discrete form R_k and Q_k given in Eqs. (2.40) and (2.41).

$$R_k = \frac{R(t)}{\Delta t} \tag{2.40}$$

$$\Upsilon_k Q_k \Upsilon_k^T = \Delta t G(t)Q(t)G^T(t) \tag{2.41}$$

It is fitting to set $G(t) = \frac{d}{dt}\Upsilon_k$. Assuming that Δt is sufficiently small, the correspondence shown in Eq. (2.42) follows.

$$\begin{aligned}G(t) = \frac{d}{dt}\Upsilon_k &\approx \frac{1}{\Delta t}\Upsilon_k \\ \Rightarrow \Upsilon_k Q_k \Upsilon_k^T &= \Delta t G(t)Q(t)G^T(t) = \Upsilon_k \frac{Q(t)}{\Delta t}\Upsilon_k^T \\ \Rightarrow Q_k &= \frac{Q(t)}{\Delta t}\end{aligned} \tag{2.42}$$

Therefore, Eqs. (2.43) and (2.44) describe directly $R(t)$ and $Q(t)$ to R_k and Q_k.

$$R(t) = \Delta t R_k \tag{2.43}$$

$$Q(t) = \Delta t Q_k \tag{2.44}$$

The description of $R(t)$ and $Q(t)$ in this fashion is useful in navigation based path planning to translate discrete problems into continuous ones and to have a more intuitive understanding in what the values represent, and therefore are used in the description of problems in this report. For the purposes of this work in which only the variance is minimized, the value of Δt does not effect the optimal path because it scales the variance by the same factor everywhere throughout the trajectory and thus does not change where the minimum occurs. This is by the same logic presented in Section 3.3.2.

Below the continuous linear Kalman filter is summarized for convenience.

Model:

$$\dot{\boldsymbol{x}}(t) = F(t)\boldsymbol{x}(t) + B(t)\boldsymbol{u}(t) + G(t)\boldsymbol{w}(t)$$
$$\tilde{\boldsymbol{y}}(t) = H(t)\boldsymbol{x}(t) + \boldsymbol{v}(t)$$

Initialize:

$$\hat{\boldsymbol{x}}(t_0) = \hat{\boldsymbol{x}}_0$$
$$P_0 = E\left\{\tilde{\boldsymbol{x}}_0\tilde{\boldsymbol{x}}_0^T\right\}$$

Gain:

$$K(t) = P(t)H^T(t)R^{-1}(t)$$

Covariance:

$$\dot{P}(t) = F(t)P(t) + P(t)F^T(t) - P(t)H(t)R^{-1}(t)H(t)P(t) + G(t)Q(t)G^T(t)$$

Estimate:

$$\hat{\boldsymbol{x}}(t_0) = \hat{\boldsymbol{x}}_0$$
$$\dot{\hat{\boldsymbol{x}}}(t) = F(t)\hat{\boldsymbol{x}}(t) + B(t)\boldsymbol{u}(t) + K(t)\left[\tilde{\boldsymbol{y}}(t) - H(t)\hat{\boldsymbol{x}}\right]$$

2.2.3 Extended Kalman Filter

The Kalman filter is the optimal estimator for linear systems, but many problems of interest, especially those in the real world, are nonlinear. The Kalman filtering technique may be adjusted to give a near optimal estimator and approximation of the error covariance. The most common approach is through the extended Kalman filter (EKF). There exists more accurate nonlinear state estimators such as the unscented

Kalman filter [18], but the EKF is used here because of its simplicity and ease of implementation.

The nonlinear system has the truth model given in Eq. (2.45).

$$\begin{aligned} \dot{\boldsymbol{x}}(t) &= \boldsymbol{f}\left(\boldsymbol{x}(t), \boldsymbol{u}(t), t\right) + G(t)\boldsymbol{w}(t) \\ \tilde{\boldsymbol{y}}(t) &= \boldsymbol{h}\left(\boldsymbol{x}(t), t\right) + \boldsymbol{v}(t) \end{aligned} \tag{2.45}$$

To arrive at the EKF, Eq. (2.45) needs to be linearized. It is assumed that the true state is sufficiently close to the estimated state. Therefore, the first-order Taylor series approximations given in Eqs. (2.46) and (2.47) can be used.

$$\boldsymbol{f}\left(\boldsymbol{x}(t), \boldsymbol{u}(t), t\right) \approx \boldsymbol{f}\left(\bar{\boldsymbol{x}}(t), \boldsymbol{u}(t), t\right) + \left.\frac{\partial \boldsymbol{f}}{\partial \boldsymbol{x}}\right|_{\bar{\boldsymbol{x}}(t), \boldsymbol{u}(t)} \left[\boldsymbol{x}(t) - \bar{\boldsymbol{x}}(t)\right] \tag{2.46}$$

$$\boldsymbol{h}\left(\boldsymbol{x}(t), \boldsymbol{u}(t), t\right) \approx \boldsymbol{h}\left(\bar{\boldsymbol{x}}(t), t\right) + \left.\frac{\partial \boldsymbol{h}}{\partial \boldsymbol{x}}\right|_{\bar{\boldsymbol{x}}(t)} \left[\boldsymbol{x}(t) - \bar{\boldsymbol{x}}(t)\right] \tag{2.47}$$

In the EKF, the nominal state $\bar{\boldsymbol{x}}$ is set to be equal to the current $\hat{\boldsymbol{x}}$. The expectations in Eq. (2.48) follow.

$$\begin{aligned} E\left\{\boldsymbol{f}\left(\boldsymbol{x}, \boldsymbol{u}(t), t\right)\right\} &= \boldsymbol{f}\left(\hat{\boldsymbol{x}}(t), \boldsymbol{u}(t), t\right) \\ E\left\{\boldsymbol{h}\left(\hat{\boldsymbol{x}}(t), t\right)\right\} &= \boldsymbol{h}\left(\hat{\boldsymbol{x}}(t), t\right) \end{aligned} \tag{2.48}$$

This leads to equations for state and measurement estimates, Eqs. (2.49) and (2.50).

$$\dot{\hat{\boldsymbol{x}}}(t) = \boldsymbol{f}\left(\hat{\boldsymbol{x}}(t), \boldsymbol{u}(t), t\right) + K(t)\left[\tilde{\boldsymbol{y}}(t) - \boldsymbol{h}\left(\hat{\boldsymbol{x}}(t), t\right)\right] \tag{2.49}$$

$$\hat{\boldsymbol{y}}(t) = \boldsymbol{h}\left(\hat{\boldsymbol{x}}(t), t\right) \tag{2.50}$$

Substituting Eqs. (2.46) and (2.47) into Eq. (2.49) using Eq. (2.45) gives the EKF structure in Eq. (2.51)

$$\dot{\tilde{\boldsymbol{x}}} = \left[F(t) - K(t)H(t)\right]\tilde{\boldsymbol{x}} - G(t)\boldsymbol{w}(t) + K(t)\boldsymbol{v}(t) \tag{2.51}$$

where:

$$F(t) \equiv \left.\frac{\partial \boldsymbol{f}}{\partial \boldsymbol{x}}\right|_{\hat{\boldsymbol{x}}(t), \boldsymbol{u}(t)} \qquad H(t) \equiv \left.\frac{\partial \boldsymbol{h}}{\partial \boldsymbol{x}}\right|_{\hat{\boldsymbol{x}}(t)} \tag{2.52}$$

This structure is equivalent to the linear Kalman filter structure Eq. (2.27), so everything else follows as from the continuous linear Kalman filter. The EKF is also summarized in the equations below.

Model:

$$\dot{\boldsymbol{x}}(t) = \boldsymbol{f}\left(\boldsymbol{x}(t), \boldsymbol{u}(t), t\right) + G(t)\boldsymbol{w}(t)$$
$$\tilde{\boldsymbol{y}}(t) = \boldsymbol{h}\left(\boldsymbol{x}(t), t\right) + \boldsymbol{v}(t)$$

Initialize:

$$\hat{\boldsymbol{x}}(t_0) = \hat{\boldsymbol{x}}_0$$
$$P_0 = E\left\{\tilde{\boldsymbol{x}}_0 \tilde{\boldsymbol{x}}_0^T\right\}$$

Gain:

$$K(t) = P(t)H^T(t)R^{-1}(t)$$

Covariance:

$$\dot{P}(t) = F(t)P(t) + P(t)F^T(t) - P(t)H^T(t)R^{-1}(t)H(t)P(t) + G(t)Q(t)G^T(t)$$
$$F(t) \equiv \left.\frac{\partial \boldsymbol{f}}{\partial \boldsymbol{x}}\right|_{\hat{\boldsymbol{x}}(t), \boldsymbol{u}(t)} \qquad H(t) \equiv \left.\frac{\partial \boldsymbol{h}}{\partial \boldsymbol{x}}\right|_{\hat{\boldsymbol{x}}(t)}$$

Estimate:

$$\dot{\hat{\boldsymbol{x}}}(t) = \boldsymbol{f}\left(\hat{\boldsymbol{x}}(t), \boldsymbol{u}(t), t\right) + K(t)\left[\tilde{\boldsymbol{y}}(t) - \boldsymbol{h}\left(\hat{\boldsymbol{x}}(t), t\right)\right]$$

3. METHODS FOR SOLVING NAVIGATION BASED PATH PLANNING PROBLEMS

3.1 General Approach

The fundamental approach to inserting the variance information into the optimal control problem is simple. The $\frac{n(n+1)}{2}$ unique elements of the covariance matrix P are appended to the state vector, and the optimization process is applied as in Section 2.1. The dynamics for these elements come from the differential matrix equation from the EKF for $\dot{P}$ given in Eq. (2.39). Instead of propagating stochastic truth and estimate values, the equation for $\dot{P}$ is calculated about the reference path. This is done assuming the estimate trajectory will closely match the reference through use of feedback controllers if applied to actual vehicles, and it results in a fully deterministic problem with smooth derivatives favorable to optimization. The matrix equation itself is expanded into the scalar equations that correspond to the unique values appended to the states. This is done to more simply derive necessary conditions and to fit in existing software. In future work, retaining the matrix form may quicken computation by reducing redundancies and using more efficient matrix multiplication algorithms. The addition of the covariance elements to the problem enables them to be incorporated into the objective functions and minimization of state estimation errors.

3.2 Addressing Problem Size

Perhaps the most significant issue to solving navigation-based problems is the curse of dimensionality that results from the addition of the covariance values. As stated before, for n stochastic vehicle states, there are $\frac{n(n+1)}{2}$ unique covariance values

each with its own costate. Furthermore, the length of the dynamic equation describing each increases by n^3 as a result of being derived from basic matrix multiplication. Each state also has a costate whose dynamics are derived from the quickly lengthening Hamiltonian. Finally, the computation work is squared in the calculation of the STM for the MSM.

The large problem size thus poses issues for quick computation and limits any user not only for the time computer resources are occupied but also to tweak problem parameters to numerically converge to a solution. Presented below are some methods that have been done to speed calculations, but more is likely needed to solve more complicated navigation problems.

3.2.1 Parallelization

Parallelization can be used to fully utilize the multiple cores of modern computer hardware. The first method shown in [19] runs the MSM in Section 2.1.2 in parallel processes distributed across the computer's separate CPU thread. Each of the multiple arcs can be propagated independently because they only need to know their initial guess and the EOM.

The problem can be further parallelized to take advantage of the hundreds of cores found in modern GPUs as shown by [9]. This method works by first propagating the states in parallel on the CPU cores as before, but especially with a fixed step propagation with K steps. A special property of the STM in Eq. (3.1) can be used to propagate it in parallel.

$$\Phi(t_2, t_0) = \Phi(t_2, t_1)\Phi(t_1, t_0) \tag{3.1}$$

Therefore, a corresponding STM $\Phi_k = \Phi(t_k, t_{k-1})$ can be calculated each time step from t_{k-1} to t_k using the already computed states. These are each computed on one of the GPU cores. Then the matrix multiplication in Eq. (3.2) is performed to compute the final STM.

$$\Phi = \Phi_K \Phi_{K-1} \dots \Phi_1 \Phi_0 \tag{3.2}$$

This multiplication can also be done with specialized algorithms for matrix multiplication on the GPU. This GPU parallelization has shown to be effective on the navigation problems more than halving computation time on the single cart problem presented later.

3.2.2 Numerical Derivatives for Costate Propagation

Another way to reduce the computation time needed is to use numerical derivations to shorten the derivatives for the costates given by Eq. (2.9). The expressions for the costates may become long when analytically computed because of the application of the chain rule so calculating the derivatives numerically is often less intensive computationally. The problems addressed in this thesis all contain functions that can handle imaginary arguments so a complex step derivative can be used and calculated using $\frac{\partial f}{\partial x} = \frac{\Im(f(x+ih))}{h}$ where h is small [20]. The terms of the Hamiltonian not dependent on the state considered because those terms do not affect the result, so the Hamiltonian used in the calculations may be reduced to $H_{\text{x terms}}$, which contains the terms in the Hamiltonian dependent on state x_i, to further reduce the calculations needed. This results in:

$$\dot{\lambda}_i = -\frac{\partial \mathcal{H}}{\partial x_i} = -\frac{\Im(\mathcal{H}(x_i + ih))}{h} = -\frac{\Im(\mathcal{H}_{\text{x terms}}(x_i + ih))}{h} \tag{3.3}$$

The benefits of using a complex step derivative over a standard forward, backward, or central difference derivative are that it only requires one function evaluation and achieve machine precision because it eliminates the subtraction that introduces truncation error. This method reduces the computation time of the derivative in single cart problem (Section 4.3) by about 50% and the derivatives in dual cart problem (Section 4.1) by about 90%. This technique is limited though by the software's ability to symbolically determine the terms contained in $H_{\text{x terms}}$. Without reducing the size of H and eliminating extraneous terms, the analytical expressions for the partial derivatives may still be shorter. The expression needs to be expanded to dissociate the states. After the unneeded terms are removed, simplification is necessary to reduce

redundant calculations. This process is computationally expensive and infeasible in some cases.

3.3 Scaling

Scaling the optimal control problem is necessary to efficiently and effectively solve an optimal control problem numerically. This is so that variables handled in the solver can be treated with the same tolerances, do not numerically dominate one another, and are independent of the physical units used to express the problem. Ideally, the problem would be scaled in such a way that all the values are close to unity. The way the solver has done the scaling in the past is to assign a scale factor to each physical unit (e.g. meter, second, kilogram). By tying the scaling of each with the physical units allows the EOM to remain dimensionally consistent without modifying them. This method applied blindly to a navigation path planning problem can cause issues though because in a realistic problem, the standard deviation of a state hopefully is orders of magnitude smaller than the state itself despite the two variables sharing the same unit. For example, in the original Two-Cart Problem presented in 1, the carts need to reach a goal 4,000 m away from their initial locations, but the standard deviation in each inter-range measurement is only 0.01 m.

3.3.1 Norm Scaling

The first method to bypass this issue involved scaling each state individually by the L^2-norm defining a scale value $k_{i,\text{norm}} = \int_0^{t_f} x_i^2 \, dt$ for state x_i. This results in a

new state vector $\boldsymbol{x}_{\text{new}}$ with dynamics defined by 3.4. The solver uses $\boldsymbol{x}_{\text{new}}$ to solve the TPBVP. The scale factors are recalculated at each continuation step to be adaptive.

$$\begin{aligned} x_i &= k_{i,\text{norm}} x_{i,\text{new}} \\ \Rightarrow \dot{\boldsymbol{x}}_{\text{new}} &= \begin{bmatrix} \frac{1}{k_{1,\text{norm}}} f_1(\boldsymbol{k}_{\text{norm}} \circ \boldsymbol{x}_{\text{new}}) \\ \vdots \\ \frac{1}{k_{n,\text{norm}}} f_n(\boldsymbol{k}_{\text{norm}} \circ \boldsymbol{x}_{\text{new}}) \end{bmatrix} \end{aligned} \tag{3.4}$$

This method was successful and allowed for solutions to be found. Unfortunately, it has several negatives which make this not the preferred method. Firstly, it requires more computations from the process in Equation 3.4. Also, special care must be taken in posing the initial guess and problem with the scaling factors in mind. Lastly, because the scaling of each state is independent from all others, two states, such as two position variables, may be scaled completely differently, which may be undesirable. For example, in the single cart problem the actual tolerance applied in the y direction may be two or three orders of magnitude higher than that applied in the x direction despite the terminal y coordinate being more difficult to target as implied by the higher variance for y.

3.3.2 Constant Scaling

Another method of overcoming the scaling issue is simply to multiply the state noise Q and measurement noise R by some factor so that the covariance elements and costates are the appropriate magnitude. Multiplying the noise by a factor k_{cov} so that $Q_{\text{new}} = k_{\text{cov}} Q$ and $R_{\text{new}} = k_{\text{cov}} R$ results in a new covariance matrix $P_{\text{new}} = k_{\text{cov}} P$ without modifying any other aspects of the problem. The consistency of this is shown in 3.5. Because the optimal path only depends on the relative sizes of the covariances

to each other and not their absolute magnitudes, the scaled problem has the same solution as the original.

$$\begin{aligned}\dot{P}_{\text{new}} &= FP_{\text{new}} + P_{\text{new}}F^T - P_{\text{new}}H^T R^{-1} H P_{\text{new}} + GQ_{\text{new}}G^T \\ &= k_{\text{cov}}FP + k_{\text{cov}}PF^T - k_{\text{cov}}PH^T \left(\tfrac{1}{k_{\text{cov}}}\right) R^{-1} H k_{\text{cov}} P + Gk_{\text{cov}}QG^T \\ &= k_{\text{cov}}\dot{P}\end{aligned} \tag{3.5}$$

A way to see that this would be true is to note that the normal states are only dependent on each other and the control but not directly on the covariance values. The control is determined by minimizing the cost functional J. The problem that minimize J and kJ where $k > 0$ are equivalent problems. By scaling the covariance elements, the problem functionally only changes by multiplying the cost function by a factor of k.

The final scaling method is an extension of this. Instead of using a scalar, more direct control can be gained by use of a matrix. A diagonal scaling matrix K is defined such that its elements are on the same order of the corresponding states' standard deviation. The relation in Eq. (3.6) defines the scaled covariance matrix P_{new}. This works well because P is composed of diagonal elements σ_i^2 and off-diagonal elements $\rho_{i,j}\sigma_i\sigma_j$ with $|\rho_{i,j}| \leq 1$, so if the matrix K is a diagonal matrix with σ_i elements, P_{new} will be made of ones on the diagonal and $\rho_{i,j}$ off-diagonal.

$$P = K_{\text{cov}}P_{\text{new}}K_{\text{cov}} \tag{3.6}$$

Applying this definition to the dynamic equation for $\dot{P}$ yields Eq. (3.8), which is used in the optimization problem.

$$\begin{aligned}\dot{P} &= K_{\text{cov}}\dot{P}_{\text{new}}K_{\text{cov}} \\ &= FK_{\text{cov}}P_{\text{new}}K_{\text{cov}} + K_{\text{cov}}P_{\text{new}}K_{\text{cov}}F^T \\ &\quad - K_{\text{cov}}P_{\text{new}}K_{\text{cov}}H^T R^{-1} H K_{\text{cov}}P_{\text{new}}K_{\text{cov}} + GQG^T\end{aligned} \tag{3.7}$$

$$\begin{aligned}\Rightarrow \dot{P}_{\text{new}} &= K_{\text{cov}}^{-1}FK_{\text{cov}}P_{\text{new}} + P_{\text{new}}K_{\text{cov}}F^T K_{\text{cov}}^{-1} \\ &\quad - P_{\text{new}}K_{\text{cov}}H^T R^{-1} H K_{\text{cov}}P_{\text{new}} + K_{\text{cov}}^{-1}GQG^T K_{\text{cov}}^{-1}\end{aligned} \tag{3.8}$$

This method may be used to bring the covariance values near to the states, and then dimensional scaling is applied.

3.4 Addressing Controls

Special consideration is merited when deciding how to express the control in a navigation based problem. The length and complexity of the differential equations may be prohibitive to symbolic computations required to find the algebraic solution to Eq. (2.13), $\frac{\partial H}{\partial u} = 0$. A method using index reduction for solving differential algebraic equations (DAE) has been effective for other problems in which a control law cannot be found explicitly [21]. This method finds an expression for the derivative of the control, $\dot{\boldsymbol{u}}$, by Eq. (3.9) and numerically integrates that instead of solving for the control directly.

$$\begin{gathered} g = \frac{\partial \mathcal{H}}{\partial u} = 0 \\ \partial_u g\left(t, \boldsymbol{x}, \boldsymbol{u}\right) \dot{\boldsymbol{u}} = -\partial_x g\left(t, \boldsymbol{x}, \boldsymbol{u}\right) \dot{\boldsymbol{x}} - \partial_t g\left(t, \boldsymbol{x}, \boldsymbol{u}\right) \end{gathered} \tag{3.9}$$

Unfortunately, for navigation based problem the length of the Hamiltonian is still prohibitive. Calculating this at every time step greatly slows computation. The most effective way to add the control is to make the control linear. This means that $\dot{\boldsymbol{x}} = F\left(t, \boldsymbol{x}\right) + B\boldsymbol{u}$. In practice, this condition may be relaxed somewhat (and will be with the control constraints) as long as the control is not embedded deeply within the states' rates and covariance matrix. The simplest way to do this if the control variable of interest is not linear is to make that original control an additional state and to make its rate equal to the new control. This requires the application of a control

constraint though so that one does not arrive trivially to the original formulation. This can be seen by Eq. (3.12) where the new control is u and the old control is w.

$$\dot{w} = u \tag{3.10}$$

$$\begin{aligned}\mathcal{H} &= \mathcal{L} + \boldsymbol{\lambda}^T f \\ &= L + \lambda_1 f_1 + \lambda_2 f_2 + \cdots + \lambda_w u + \ldots \lambda_n f_n \\ &= \mathcal{H}_0 + \lambda_w u\end{aligned} \tag{3.11}$$

$$\frac{\partial \mathcal{H}}{\partial u} = \lambda_w = 0 \tag{3.12}$$

$$\frac{\partial \mathcal{H}}{\partial w} = -\dot{\lambda}_w = -\frac{d}{dt}\,0 = 0 \tag{3.13}$$

The condition $\frac{\partial H}{\partial w} = 0$ still has to be held and the control needs to be found numerically to hold $\lambda_w = 0$. The way to apply a linear control without these issues is to apply a control constraint. In traditional OCT, the minimum principle (Eq. (2.14)) can be used to find the control.

3.4.1 Control Bounding

Traditionally, adding control constraints to an optimal control problem required prior knowledge of the existence and sequence of constrained and unconstrained arcs, so the trajectory can be appropriately divided into multiple arcs and the correct control being applied using the minimum principle Eq. (2.14) [16]. The requirement for that knowledge of the system a priori prevents the application of the traditional method to the problems presented here.

Instead, the control constraints shown in this report were all implemented using the Epsilon-Trig Regularization Method [13]. The main benefits to bounding the control this way are that the problem can be solved using a single arc and that it is relatively simple to implement. The method requires replacing the control u with the trigonometric function $u_{max} \sin u_{\triangle}$, which is clearly bounded between $\pm u_{max}$. The optimal control problem is then solved with $u_{\triangle}$ as the control. It is also required to add an error term to regularize discontinuities in the control law which would

prevent propagating the differential equations. As originally presented, the error term $\epsilon u_{max} \cos u_{\triangle}$ was added to an arbitrary state's rate. The constant ϵ should be made small relative to the problem, and as ϵ approaches 0, the regularized problem's solution approaches that of the original problem. The approach is shown in Eq. (3.14).

$$\begin{aligned} |u| \leq u_{max} \qquad & u = u_{max} \sin u_{\triangle} \\ \dot{x}_i = f_i \qquad \longrightarrow \quad & \dot{x}_i = f_i + \epsilon u_{max} \cos u_{\triangle} \\ \mathcal{H} = \mathcal{L} + \boldsymbol{\lambda}^T f \qquad & \mathcal{H} = \mathcal{L} + \boldsymbol{\lambda}^T f + \lambda_i \epsilon u_{max} \cos u_{\triangle} \end{aligned} \tag{3.14}$$

Though the original formulation was used for some of the results presented here, adding the error term to a state's dynamics is not ideal. Firstly, modifying the state dynamics may result in constraints that are satisfied in the new system to not be satisfying in the original system with the same control law. Furthermore, the regularized control law will be strongly dependent on λ_i, which is problematic if λ_i changes magnitude greatly (changing the effect of the term significantly) or goes to 0 (eliminating the regularization entirely). Both these problems can be resolved by noticing that the error term can be added to the Hamiltonian in almost an identical way but without the dependency on λ_i by subtracting it from the path cost L. Subtraction is chosen so that minimizing the path cost results in $|u\triangle| \leq \pi/2$. This results in Eq. (3.15). Sizing ϵ is easier with this method as it can be sized with respect to the cost only without taking into account of its effect on a state.

$$\begin{aligned} |u| \leq u_{max} \qquad & u = u_{max} \sin u_{\triangle} \\ J = \phi + \int_{t_0}^{t_f} L \, dt \longrightarrow \quad & J = \phi + \int_{t_0}^{t_f} \mathcal{L} - \epsilon u_{max} \cos u_{\triangle} \, dt \\ \mathcal{H} = L + \boldsymbol{\lambda}^T f \qquad & \mathcal{H} = \mathcal{L} - \epsilon u_{max} \cos u_{\triangle} + \boldsymbol{\lambda}^T f \end{aligned} \tag{3.15}$$

3.4.2 Added Nonlinearity Due to Control Bounding

By bounding the control, the nonlinearity present in the problems worsens, and it may render certain problems nearly unsolvable. Some symptoms of these problems

are that often the root solver will reduce the residuals to be fairly close to zero only to have them suddenly grow very large or that the propagation will break from radically changing derivatives. The issues seem to worsen when areas develop where the problem becomes relatively insensitive to the control which particularly pertains to navigation problems as demonstrated in Section 4.3.3. It may be thought that this insensitivity to the control is the only issue, but this is incongruent with the problem exhibiting with the sudden changes in the solver's behavior. Instead, the issues arise from the presence of sensitive and insensitive regions together.

A bounded Zemelo's problem described in Eqs. (3.16) to (3.19) is used to demonstrate this. The problem displayed has already been converted to use Epsilon-Trig method bounding. This problem is dynamically equivalent to the single-cart problem in Section 4.3 without the covariance dynamics.

$$\min J = \int_0^{t_f} (1 + \epsilon u_{max} \cos u_{\triangle}) dt \tag{3.16}$$

$$\boldsymbol{x} = \begin{bmatrix} x \\ y \\ \theta \end{bmatrix}, \qquad f(\boldsymbol{x}) = \begin{bmatrix} v \cos\theta \\ v \sin\theta \\ u_{max} \sin u_{\triangle} \end{bmatrix} \tag{3.17}$$

With boundary conditions and parameters:

$$x_0 = 0, \qquad y_0 = 0, \qquad \theta_0 = 0, \qquad x_f = 10, \qquad y_f = 5 \tag{3.18}$$

$$v = 1, \qquad u_{max} = 0.1, \qquad \epsilon = 0.1 \tag{3.19}$$

It is helpful here not to look at the sensitivity of the objective to the control, but rather, observe the effect that the free initial costate values have on the fixed terminal values. This is because the initial values are what the TPBVP solver using shooting methods directly adjusts to satisfy the boundary conditions. Therefore, these sensitivities determine whether the solver can find a solution. In bounded problems, there is often not a sensitivity issue between the control and objective, as can be observed at times with the relative ease in solving unbounded variants. Instead, the

issue is between the costates and the control, causing the insensitivity between the costates and the states. The bounding creates this in that near the control bounds, larger magnitude costate values only bring the control asymptotically closer to the constraint, so as the control approaches the bound, the costates have lesser effect. Section 3.4.2 shows the corresponding effects of varying the initial costates $\lambda_{x,0}$ and $\lambda_{\theta,0}$ about the optimal solution on the final states. For reference to the optimal, $\lambda^{\star}_{x,0} = -0.7799$ and $\lambda^{\star}_{\theta,0} = -2.200$. Most notable in the plots is the change in magnitude of the derivatives in the lower plots. These trends are similar to what is seen in the arctangent function which is known to be difficult to root solve. If the current solution is in a "flat" region, where large changes in initial value result only in small changes in terminal values, the solver will attempt to take a very large step and likely overshoot the solution significantly. Furthermore, the condition number of the STM, and Jacobian by extension, spikes around the optimal solution indicating that the problem is near-singular there. Theoretically, a first order method should be able to converge to a solution with a singular Jacobian, but significantly slower. Unfortunately, in practice, a bad step often results in failed state propagation, which either instantly break the solver or starts a series of degrading quality steps that cannot converge.

Control constraints like those used here require special care to reliably obtain results. Knowing how the addition of the constraint impacts the search space allows the researcher to better diagnose numerical issues, select smoothing parameters, and develop continuation strategies.

3.4.3 Control Energy Cost: Alternative to Control Bounding

An alternative to control bounding to use linear controls is to add a control "energy" path cost. Equation (3.20) shows the added path cost.

$$L_{\text{con}} = k_{\text{en}} u^2,\ k_{\text{en}} > 0 \tag{3.20}$$

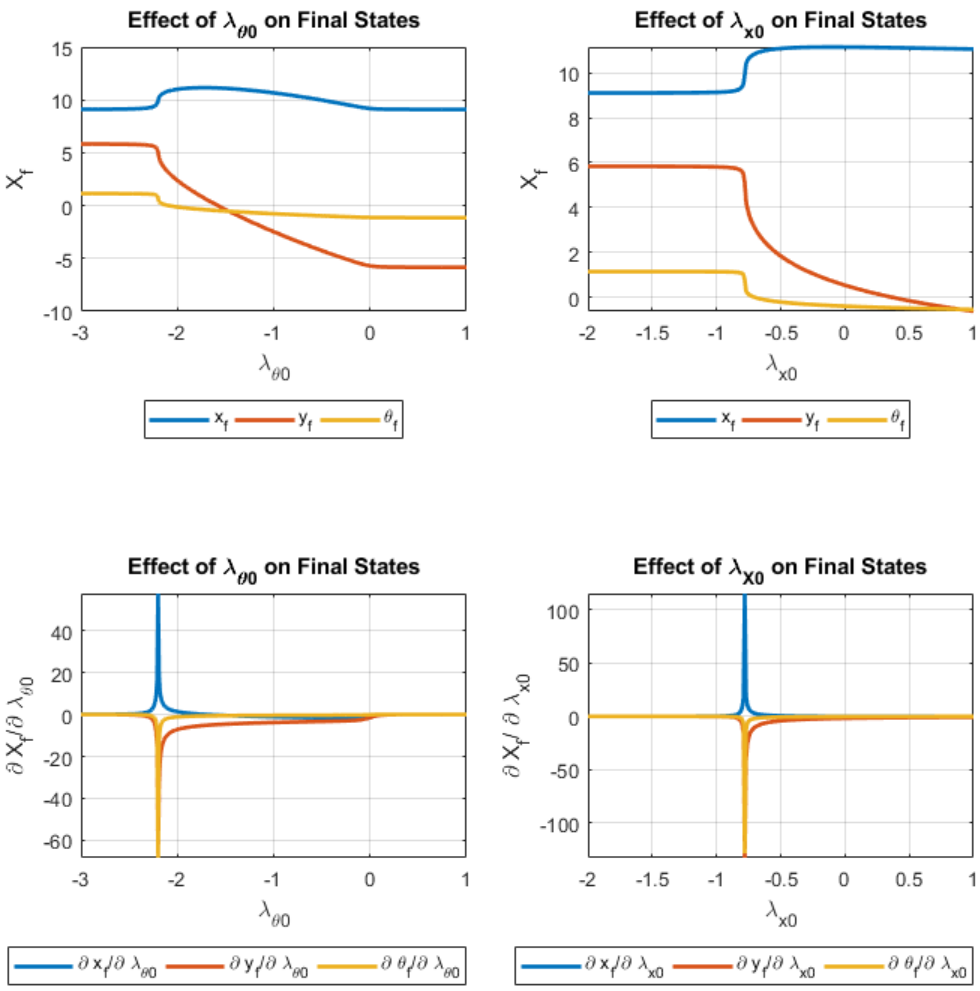

Figure 3.1. Numerical Investigations into Sensitivities of Bounded Zemelo Problem to Initial Costates

Applying Eq. (2.13) results in the simple control law for these problems in Eq. (3.21) where $\dot{x}_u = u$.

$$\begin{aligned} \frac{\partial H}{\partial u} &= \frac{\partial \left(L_{\text{con}} + \lambda_{x_u} u \right)}{\partial u} = 2k_{\text{en}} u + \lambda_{x_u} = 0 \\ \rightarrow \; u &= -\frac{\lambda_{x_u}}{2k_{\text{en}}} \end{aligned} \tag{3.21}$$

The reason that the control bounding method is presented as the primary method is that it is easier to intuitively understand, retains the pure variance cost, and relates directly to actual constraints native to the problems, such as the single cart problem (Section 4.3). One benefit to the control energy cost method is that it does not create new infeasible regions of the design space. Moreover, it does not appear to suffer as much from the nonlinearity discussed in Section 3.4.2. Lastly, if all that is desired from the designer is a decrease of the extreme control effort, this method will lead the optimizer to "distribute" the limited control where it is most useful to minimize the variance.

4. SOLUTIONS TO NAVIGATION BASED PROBLEMS

This chapter applies the methods described above to particular navigation based problems. The first two problems presented, the dual-cart problem and the 1-D train problem, provide an insight into characteristics of problems of this type and as a starting point to developing the tools further. The second two problems, the single cart problem and aircraft descent problem, were successfully solved and fulfill the goal of this thesis.

4.1 Dual Cart Problem

As mentioned in Chapter 1, the dual cart problem, studied in [5, 6], served as the primary motivating problem for the work in this thesis, so it is described mathematically in Eqs. (4.1) to (4.5) with a diagram shown in Fig. 4.1. The parameters given below correspond to a discrete time estimator to match the original papers. It would need to be converted to a near equivalent continuous time estimator using Eqs. (2.43) and (2.44). The two carts, separated initially by 600 m, travel to their respective goals 4,000 m downrange. The objective is to minimize the variance in terminal estimation. The best performing trajectories from [5] and [6] are given in Figs. 4.2(a) and 4.2(b) respectively.

$$\min J = p_{x_1x_1}(t_f) + p_{y_1y_1}(t_f) + p_{x_1x_1}(t_f) + p_{y_2y_2}(t_f) \tag{4.1}$$

Subject to:

$$\boldsymbol{u} = \begin{bmatrix} \omega_1 \\ \omega_2 \end{bmatrix} \qquad \boldsymbol{x} = \begin{bmatrix} x_1 \\ y_1 \\ \theta_1 \\ x_2 \\ y_2 \\ \theta_2 \end{bmatrix} \qquad \boldsymbol{f} = \begin{bmatrix} \dot{x_1} \\ \dot{y_1} \\ \dot{\theta_1} \\ \dot{x_2} \\ \dot{y_2} \\ \dot{\theta_2} \end{bmatrix} = \begin{bmatrix} v\cos\theta_1 \\ v\sin\theta_1 \\ \omega_1 \\ v\cos\theta_2 \\ v\sin\theta_2 \\ \omega_2 \end{bmatrix} \tag{4.2}$$

$$|\omega| \leq \omega_{\max}, \qquad \Psi_0 = \begin{bmatrix} x_1(0) - 0\,\mathrm{m} \\ y_1(0) - 0\,\mathrm{m} \\ x_2(0) - 0\,\mathrm{m} \\ y_2(0) - 600\,\mathrm{m} \end{bmatrix} = \mathbf{0}, \qquad \Psi_f = \begin{bmatrix} x_1(t_f) - 4000\,\mathrm{m} \\ y_1(t_f) - 0\,\mathrm{m} \\ x_2(t_f) - 4000\,\mathrm{m} \\ y_2(t_f) - 600\,\mathrm{m} \end{bmatrix} = \mathbf{0} \tag{4.3}$$

With measurement:

$$\boldsymbol{h} = \rho = \sqrt{(x_1 - x_2)^2 + (y_1 - y_2)^2} \tag{4.4}$$

With parameters:

$$\begin{aligned} v = 30\,\mathrm{m/s}, \qquad \omega_{\max} = 1\,\mathrm{rad/s}, \qquad \Delta t = 0.1\,\mathrm{s} \\ \sigma_v = 0.01\,\mathrm{m/s}, \qquad \sigma_\omega = 0.01\,\mathrm{rad/s}, \qquad \sigma_\rho = 0.01\,\mathrm{m} \end{aligned} \tag{4.5}$$

The greatest barrier to solving this problem using optimal control theory is its computational burden. Despite very simple state dynamics, the additional dynamics needed for both the EKF and subsequent OCT quickly become immense. Firstly, the 6 original physical states require the $\frac{6(6+1)}{2} = 21$ unique covariance elements. The original states and covariance elements all need their corresponding costate values requiring the propagation of 54 ordinary differential equations. Moreover, the size of the differential equations vastly grows for each additional set of dynamics. The matrix operations for the state estimation increase roughly by n^3. Therefore, the state estimation for the dual cart requires about eight times the computations than

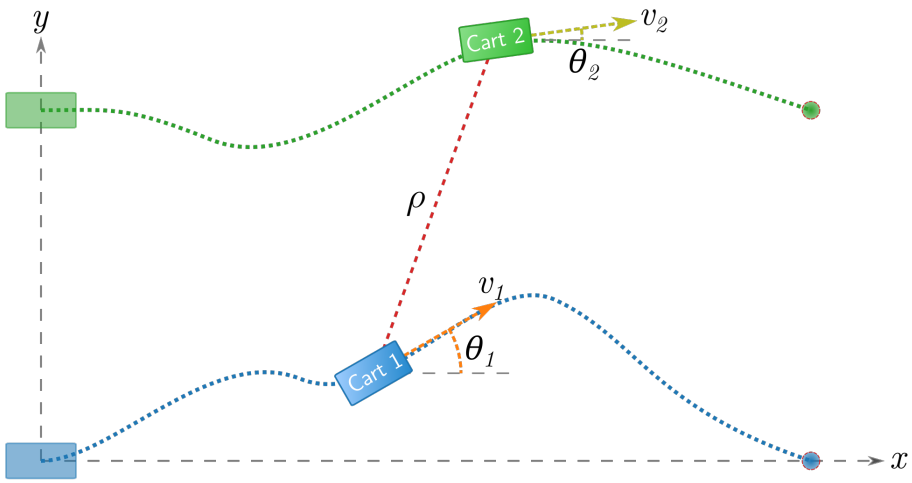

Figure 4.1. Diagram of Dual Cart Problem

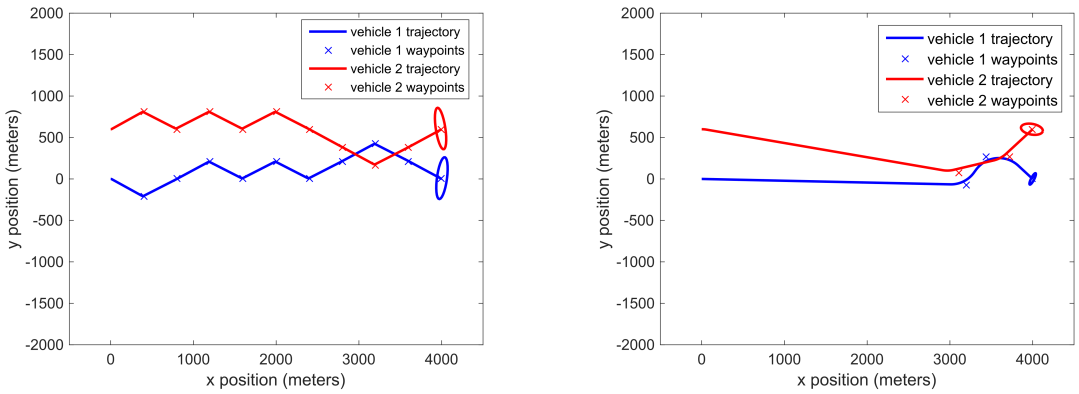

(a) Best Trajectory From [5]

(b) Best Trajectory From [6]

Figure 4.2. Previously Obtained Results for Dual Cart Problem

the single cart problem in Section 4.3. Worse still, the calculations for the costate dynamics, which are described by $\boldsymbol{\lambda} = -\frac{\partial H}{\partial x} = -\frac{\partial}{\partial x}\left(L + \boldsymbol{\lambda}^T \boldsymbol{f}\right)$, become much larger as the previously mentioned dynamics grow because those are contained within the vector $\boldsymbol{f}$. The time needed to simply propagate the ordinary differential equations prohibits effectively solving this problem without special considerations. This is why the remaining sections focus on smaller problems, but including further computational optimizations and avoiding the possible pitfalls shown in Sections 4.2 and 4.3.3 should enable this problem to be solved as future work.

4.2 1-D Train Problem

As shown, the complexity of the navigation based path planning problems grows very quickly with the number of states. When the complexity of the problem is too great, it is difficult to determine what may prevent finding solutions. The differential equations for the covariance values in a non-matrix form are usually very long even for problems that appear relatively simple. This inhibits the ability to intuitively understand how the solutions would behave by inspection of the differential equations. To gain a more fundamental understanding, one of the simplest problems of this type

was examined. It consists of a vehicle that can move only in one direction with instantaneous acceleration. It may be helpful to imagine the vehicle as an electric model train. The train measures a bearing angle from a beacon located at (x_b, y_b) off one side of the track. There is uncertainty in measuring the bearing angle β and the train's velocity, u, and an EKF estimates the state x. The bearing angle β is calculated with the function $\arctan2\,(y, x)$, which returns the angle between the positive x-axis and the line the connects the origin to the coordinates (x, y). For the computations in this thesis, $\arctan2\,(y, x)$ obtains equivalent results as the standard inverse tangent function $\tan^{-1}(\frac{y}{x})$, but it more closely describes the bearing angle β because it can return values for all four quadrants. Velocity is the control and is bounded. For the discussion, the methods presented in Section 3.4.1 or Section 3.4.3 were not applied because this problem can be solved by introspection. Figure 4.3 shows a diagram of the problem. It is described mathematically in Eqs. (4.6) and (4.7).

$$\dot{x}(t) = u + w \tag{4.6}$$

$$\tilde{y}(t) = \beta + v = \arctan2\,(y_b, x_b - x) + v \tag{4.7}$$

where:

$$\begin{aligned} 0 \leq u \leq u_{max} \\ w(t) \sim \mathcal{N}(0, \sigma_u^2) \\ v(t) \sim \mathcal{N}(0, \sigma_\beta^2) \end{aligned} \tag{4.8}$$

$$P(t) = [p_{11}]$$

$$F(t) \equiv \left.\frac{\partial f}{\partial x}\right|_{\hat{x}(t), \hat{u}(t)} = 0 \tag{4.9}$$

$$H(t) \equiv \left.\frac{\partial h}{\partial x}\right|_{\hat{x}(t)} = \frac{y_b}{(x_b - x)^2 + y_b^2}$$

$$\Rightarrow \dot{P}(t) = \dot{p}_{11} = \sigma_u^2 - p_{11}^2 \frac{y_b^2}{\sigma_\beta^2((x_b - x)^2 + y_b^2)^2} \tag{4.10}$$

The differential equation for the variance of the train's location p_{11}, shown in Eq. (4.10), is now simple enough to examine directly. Considering that σ_u, σ_ϕ, x_b,

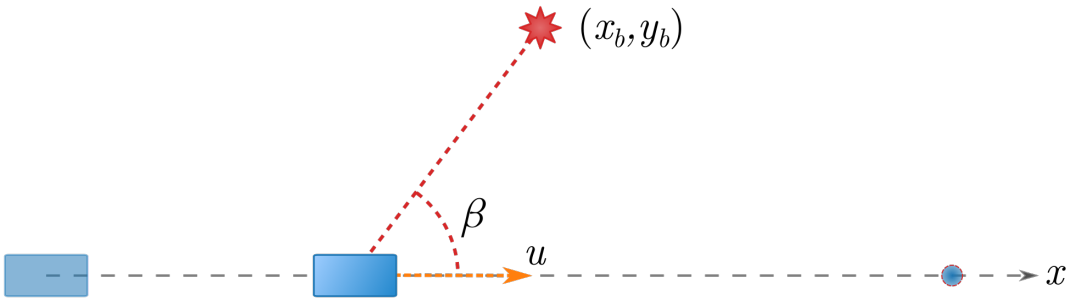

Figure 4.3. 1-D Train Problem Diagram

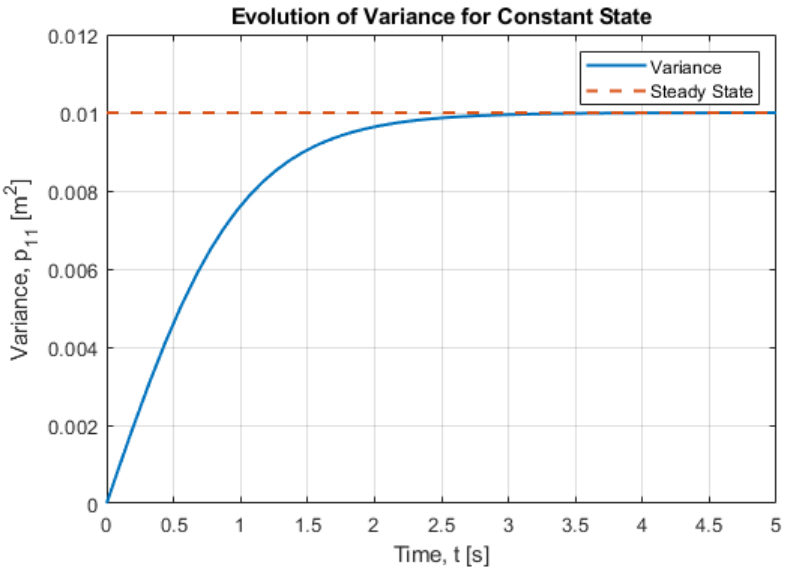

Figure 4.4. Convergence of Variance of Non-Moving Train

and y_b are constant, a steady-state value for p_{11} can be calculated for a given location for a train that is not moving (Eq. (4.11)).

$$\begin{aligned} \dot{p}_{11} &= c_0 - p_{11}^2 c_1(x) \\ c_0 &> 0 \\ p_{11}^2 c_1(x) &> 0 \\ \Rightarrow \lim_{t\to\infty} p_{11}(x,t) &= \sigma_u \sigma_\beta \frac{y_b^2 + (x_b - x)^2}{y_b} \end{aligned} \tag{4.11}$$

This asymptotic behavior is shown in Figure 4.4 for the case where $x_b = 5\,\text{m}$; $y_b = 1\,\text{m}$; $\sigma_\beta = 0.1\,\text{rad}\sqrt{\text{s}}$; $\sigma_u = 0.1\,\frac{\text{m}}{\sqrt{\text{s}}}$ at $x = 5\,\text{m}$. This also suggests that one can find a minimum steady state variance based on location. For this example, this is when the train is closest to the landmark. This behavior's effect can be seen throughout the trajectory. The dotted line in Figure 4.5 shows the steady-state values along the path. Also in Figure 4.5 are plotted the variance for different constant velocities. The variance values increase if they are below the steady state line and decrease if they are above it as would be expected.

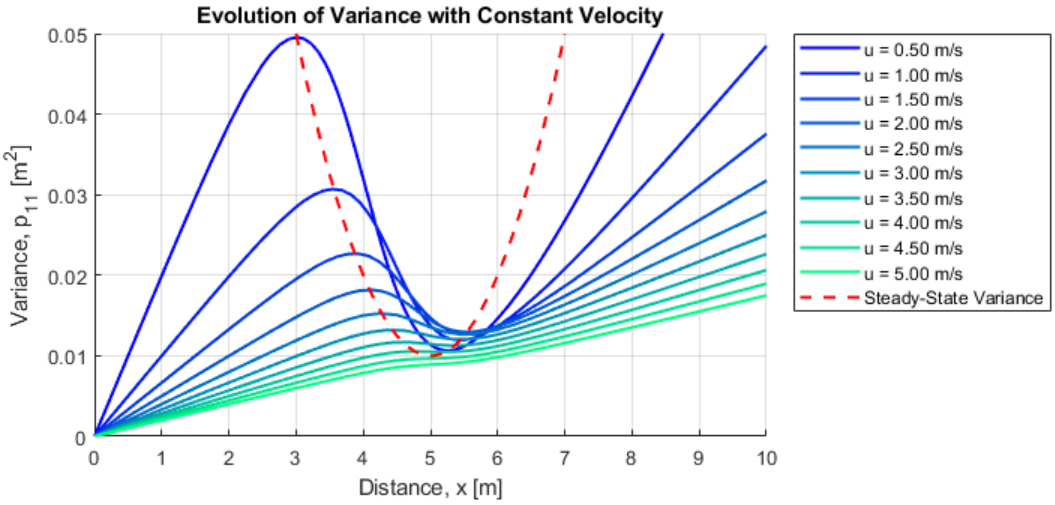

Figure 4.5. Variance Location of Train with Constant Velocity

Simply propagating the problem's equations forward provided much insight into the nature of the problem. Perhaps the most significant discovery is that if the objective is to minimize variance and the maximum velocity is below about 4.5 m/s, the problem has infinitely many optimal solutions that theoretically take infinite time to complete. If the maximum velocity is large enough, the optimal solution is to simply go as fast as possible to the end to minimize the time the variance has to grow. If the train cannot go fast enough to prevent the variance from exceeding the "steady-state" value, the issues arise. The optimal solution then is to go closest to the landmark using any velocity profile (infinitely many solutions), stop, wait infinitely long for the variance to reach the lowest "steady-state" value, and finally go at maximum speed to the end. This simple example shows that these issues can occur, which both would prevent finding a solution with the optimal control theory solver. Using more complicated objective functions, such as one that includes time, or implementing further constraints on the system may prevent these issues from appearing.

The similar problem found in [1] used the control energy path cost instead of the strict control bounds and also placed a constraint on the final time. It also did not examine the vehicle as it crosses the beacon, important for this discussion above. The results obtained there are consistent with the case presented here. Notably, as the relative weight of the control cost was decreased, the velocity control concentrated with greater magnitude towards the end of the allotted time. In other words, the vehicle remained as close to the beacon for as long as possible given the specified control cost and time constraint. Furthermore, the covariance value may be seen to converge to a common value near the beacon as seen above.

4.3 Single Cart Problem

The single cart problem presented below is a reduced version of the motivating dual-cart problem. A stationary beacon with a known location replaces the second

cart. Like the dual-cart problem, the "cart" can be viewed as any turn-limited, fixed vehicle moving within a 2-D plane such as a fixed-altitude UAV. This problem is simple enough to be solved within a reasonable time without the trivial or infinite time solutions of the very simple 1-D problem.

4.3.1 Problem Formulation

The equations describing the problem are given in Eqs. (4.12) to (4.22), and Fig. 4.6 displays a diagram. The cart is to move from its initial location and orientation to a goal position downrange with a bounded turn-rate being the control. The objective is to minimize the terminal location estimation error. The beacon from which it takes a range measurement is placed halfway downrange between the initial and terminal location and offset by some crossrange distance. The measurement contains random noise as well as random noise corresponding to the vehicle's speed and turn rate. The nominal parameters are given in Eq. (4.22).

$$\min J = p_{xx}(t_f) + p_{yy}(t_f) \tag{4.12}$$

Subject to:

$$\boldsymbol{f} = \begin{bmatrix} \dot{x} \\ \dot{y} \\ \dot{\theta} \end{bmatrix} = \begin{bmatrix} v\cos\theta \\ v\sin\theta \\ \omega \end{bmatrix} \tag{4.13}$$

$$|\omega| \leq \omega_{\max}, \qquad \Psi_0 = \begin{bmatrix} x(0) - 0\,\mathrm{m} \\ y(0) - 0\,\mathrm{m} \\ \theta(0) - 0\,\mathrm{deg} \end{bmatrix} = \mathbf{0}, \qquad \Psi_f = \begin{bmatrix} x(t_f) - x_f \\ y(t_f) - y_f \end{bmatrix} = \mathbf{0} \tag{4.14}$$

With measurement:

$$\boldsymbol{h} = \rho = \sqrt{(x - x_b)^2 + (y - y_b)^2} \tag{4.15}$$

With covariance dynamics:

$$\dot{P} = FP + PF^T - PHR^{-1}H^TP + GQG^T \tag{4.16}$$

$$Q = \frac{E\left\{\boldsymbol{w}(t)\boldsymbol{w}^T(\tau)\right\}}{\delta\left(t-\tau\right)} = \begin{bmatrix} \sigma_v^2 & 0 \\ 0 & \sigma_\omega^2 \end{bmatrix} \tag{4.17}$$

$$R = \frac{E\left\{\boldsymbol{v}(t)\boldsymbol{v}^T(\tau)\right\}}{\delta\left(t-\tau\right)} = \begin{bmatrix} \sigma_\rho^2 \end{bmatrix} \tag{4.18}$$

$$F = \frac{\partial \boldsymbol{f}}{\partial \boldsymbol{x}} = \begin{bmatrix} 0 & 0 & -v\sin\theta \\ 0 & 0 & v\cos\theta \\ 0 & 0 & 0 \end{bmatrix} \tag{4.19}$$

$$H = \frac{\partial \boldsymbol{h}}{\partial \boldsymbol{x}} = \begin{bmatrix} \frac{(x-x_b)}{\sqrt{(x-x_b)^2+(y-y_b)^2}} & \frac{(y-y_b)}{\sqrt{(x-x_b)^2+(y-y_b)^2}} & 0 \end{bmatrix} \tag{4.20}$$

$$G = \begin{bmatrix} \cos\theta & 0 \\ \sin\theta & 0 \\ 0 & 1 \end{bmatrix} \tag{4.21}$$

With parameters:

$$\begin{gathered} v = 30\,\mathrm{m/s}, \qquad \omega_{\max} = 0.1\,\mathrm{rad/s} \\ \sigma_v = 0.1\,\mathrm{m}/\sqrt{\mathrm{s}}, \qquad \sigma_\omega = 0.1\,\mathrm{rad}/\sqrt{s}, \qquad \sigma_\rho = 0.1\,\mathrm{m}\sqrt{s} \\ x_b = x_f/2, \qquad y_b = 50\,\mathrm{m} \end{gathered} \tag{4.22}$$

4.3.2 Results

The results for the nominal single-cart are shown in Fig. 4.7. The terminal down-range distance was set to 1,000 m. For this problem, solving longer trajectories becomes infeasible because of the issues discussed in Section 4.3.3. By modifying the path, the variance in the terminal location is reduced from $47.2\,\mathrm{m}^2$ of the straight path to $1.84\,\mathrm{m}^2$, a 96% reduction. The optimal path turns away from the beacon and follows a curved path to the goal. The control, ω, is near the control constraint only near the beginning of the trajectory, indicating that the inclusion of the constraint does not affect the trajectory significantly.

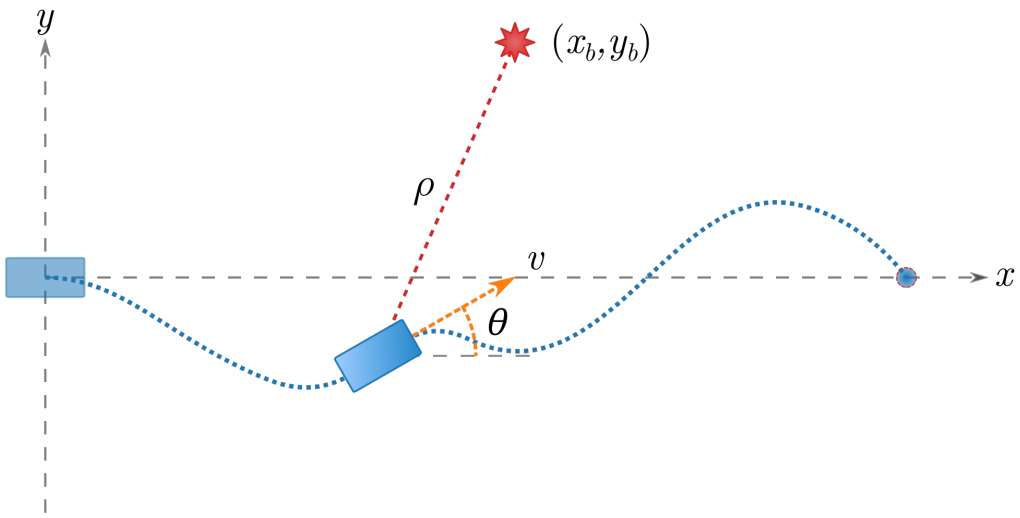

Figure 4.6. Diagram of Single Cart Problem

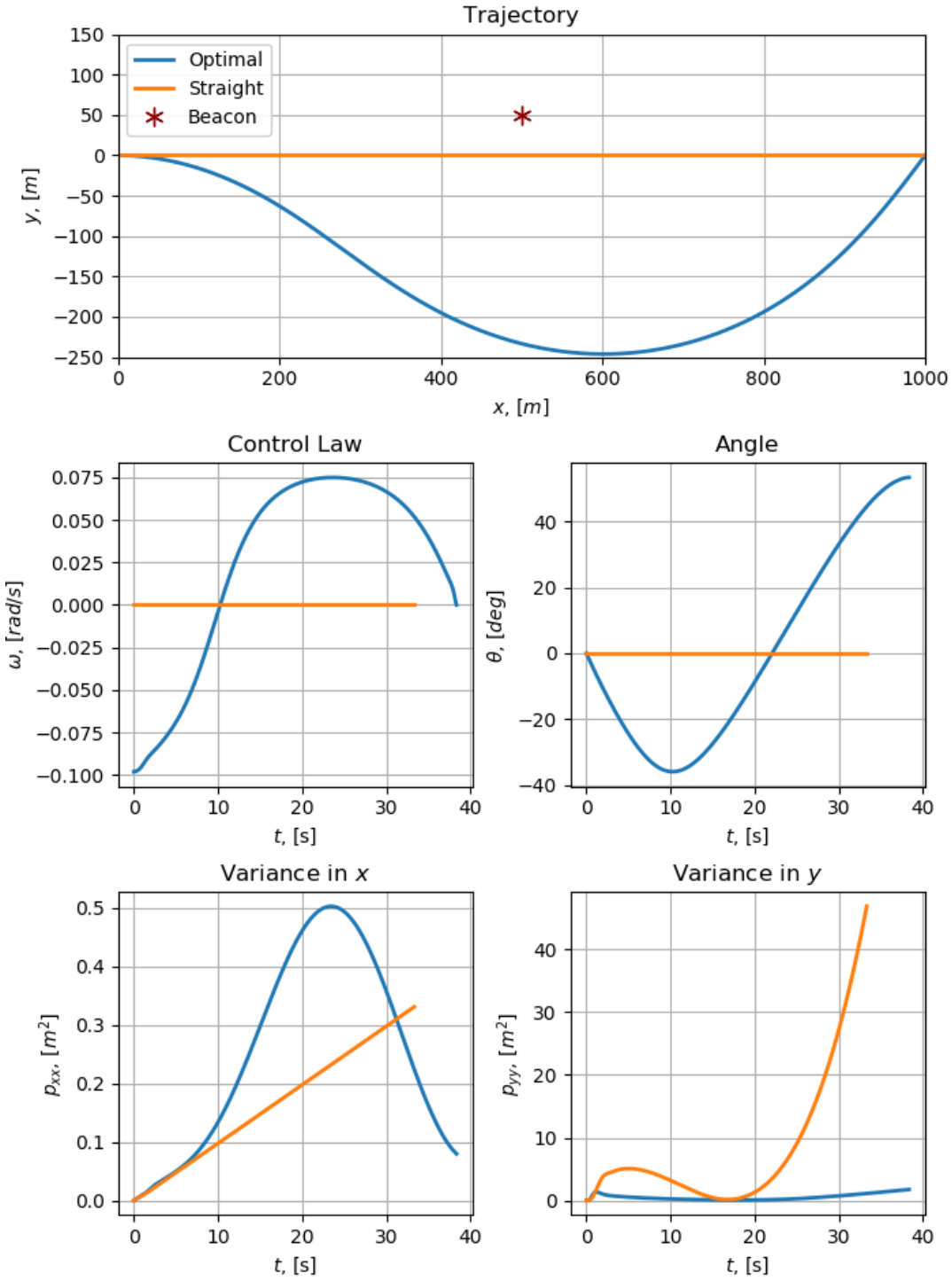

Figure 4.7. Results of Single Cart Problem to Minimize Terminal Covariance

One goal of this research is to uncover the reasons that some trajectories result in lower variance than others. Firstly, the variance of the crossrange y, p_{yy}, dominates the variance in location by more than an order of magnitude. This is partly because the angle θ is often small so that deviations in θ have a greater relative effect to crossrange y than to downrange x. The path is thus changed mostly to minimize p_{yy} over p_{xx}.

Minimizing the elements of P corresponds to minimizing the elements of $\dot{P}$, so its helpful to look at Eq. (4.28), $\dot{P} = FP + PF^T - PH^T R^{-1} HP + G^T QG$. The direct contribution of the state dynamics, $FP + PF^T$ does not vary with the vehicle's location. Therefore, investigating the term dependent on the measurement, $-PH^T R^{-1} HP$, in Eq. (2.39) is key to find the relationship between the trajectory and variance. The term $PH^T R^{-1} HP$ is positive semidefinite (and positive definite if PH has full rank) because R^{-1} is positive definite. As a result, increasing the magnitude of the elements in H will make $-PH^T R^{-1} HP$ more negative, which is desirable. Of elements in H, $\frac{\partial h}{\partial y}$ that relates h to y is the most important because it relates most closely to p_{yy}. As a result, the optimal path has the vehicle maximizing the magnitude $\frac{\partial h}{\partial y}$. This is reasonable because $\frac{\partial h}{\partial y}$ is the degree to which the state y changes the measurement h. In other words, it is representative of the correspondence between h and y.

The upper plot in Fig. 4.8 shows a surface of $\frac{\partial h}{\partial y}$. The optimal trajectory to 200 m downrange guides the cart to travel where $\frac{\partial h}{\partial y}$ is minimized (maximizing $\left|\frac{\partial h}{\partial y}\right|$) and thus supports the heuristic. Observing that the magnitude p_{yy} is lowest when in that region corroborates it further. If the vehicle turned the other direction, the vehicle would have to travel more in the area where $\frac{\partial h}{\partial y}$ is near zero.

Changing the measurement type provides more evidence for the heuristic. A relative bearing measurement, $h = \beta = \arctan 2(x - x_b, y - y_b)$, with standard deviation $\sigma_\theta = 0.1\,\mathrm{deg}\sqrt{\mathrm{s}}$ replaces the range measurement for a trajectory in Fig. 4.9. Instead of turning to the right like the vehicle with the range measurement, it turns to the left. The behavior is consistent with the corresponding plot in Fig. 4.8. There is also a spike in the variance p_{yy} when the cart passes the downrange location of the beacon

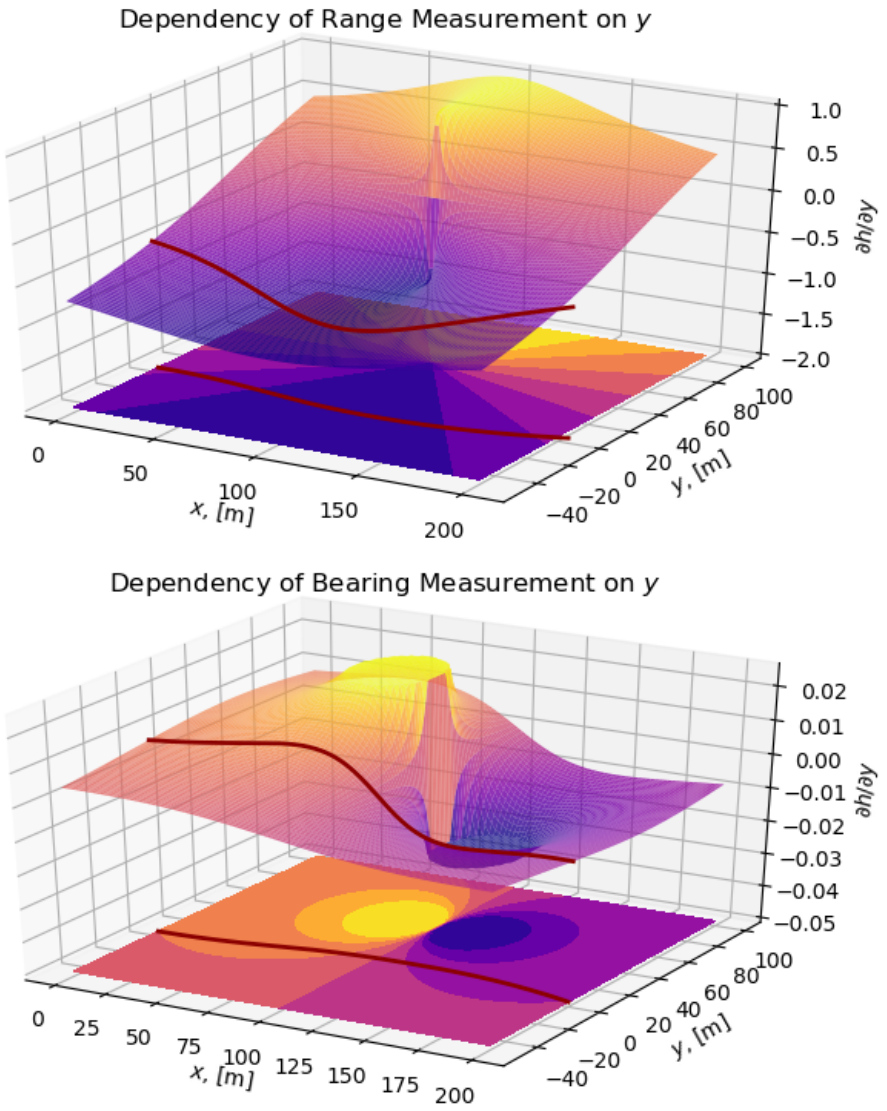

Figure 4.8. Dependency of Measurements on y as Function of Location

around where $\frac{\partial h}{\partial y} = 0$. This explanation explains that the optimal trajectory with a range measurement moves the vehicle away from the beacon, but the variance is lowest when closest to the beacon, and vis-a-versa with a bearing measurement.

4.3.3 Sensitivity to Control

The first issue related to sensitivity/insensitivity to the control was already covered in Section 3.4.2. The second is related more directly to the problem itself. That is the way the value of p_{yy} is "squeezed" as the cart passes the beacon. As noted earlier, this can be seen in Figs. 4.7 and 4.9 as the variance reaches a minimum. This minimum is bounded from below so there is a tendency for the variance to approach the same value regardless of trajectory. Figure 4.10 demonstrates this by showing various cart paths that all end at the same point with virtually identical terminal variances. This echoes what was observed in the electric train problem (Section 4.2). In problems to minimize terminal variance, the convergence of the objective states means that there can be any control history prior to the midpoint and still have a nearly optimal trajectory. Ultimately, this prevents finding a solution because the insensitivity leads to many numerical issues. This can be avoided in future work by identifying such points and beginning the optimization from them. Identifying this issue explains why the path cost variant of the problem, where $J = \int_0^{t_f} p_{11} + p_{22}\, dt$, is able to converge to a solution with longer trajectories and with fewer apparent numerical issues because the initial portion of the trajectory contributes directly to the total cost. Still, the path cost variant can suffer from the insensitivity seen by the flatness of derivative $\frac{\partial H}{\partial y}$ in Fig. 4.8 around the middle portion of the trajectory for the range problem and at the ends for the bearing problem. Figure 4.11 demonstrates that in this region, the left-right distance of the cart to the beacon makes only a small change to the variance p_{yy}.

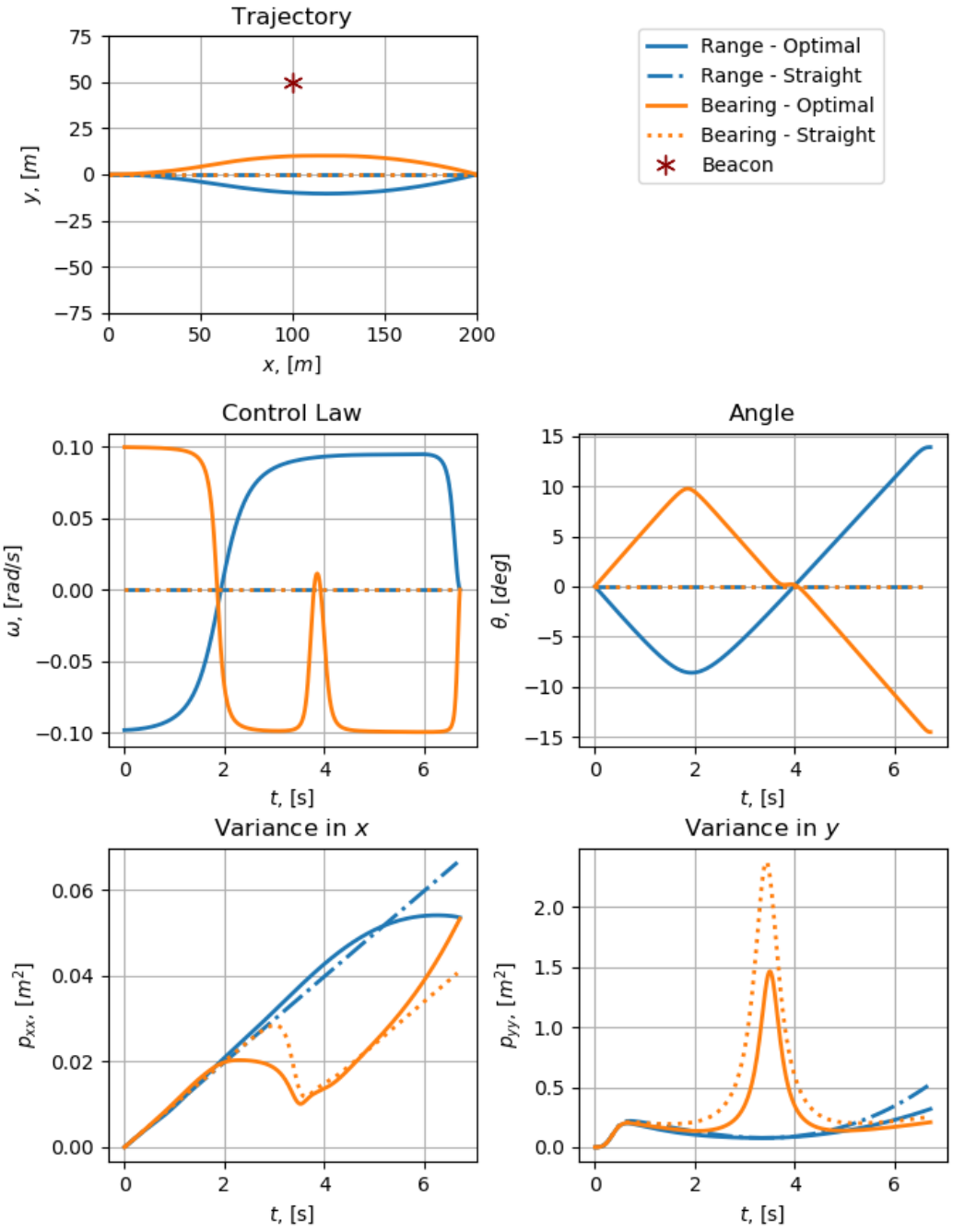

Figure 4.9. Comparison Between Solutions With Range and Bearing Measurements

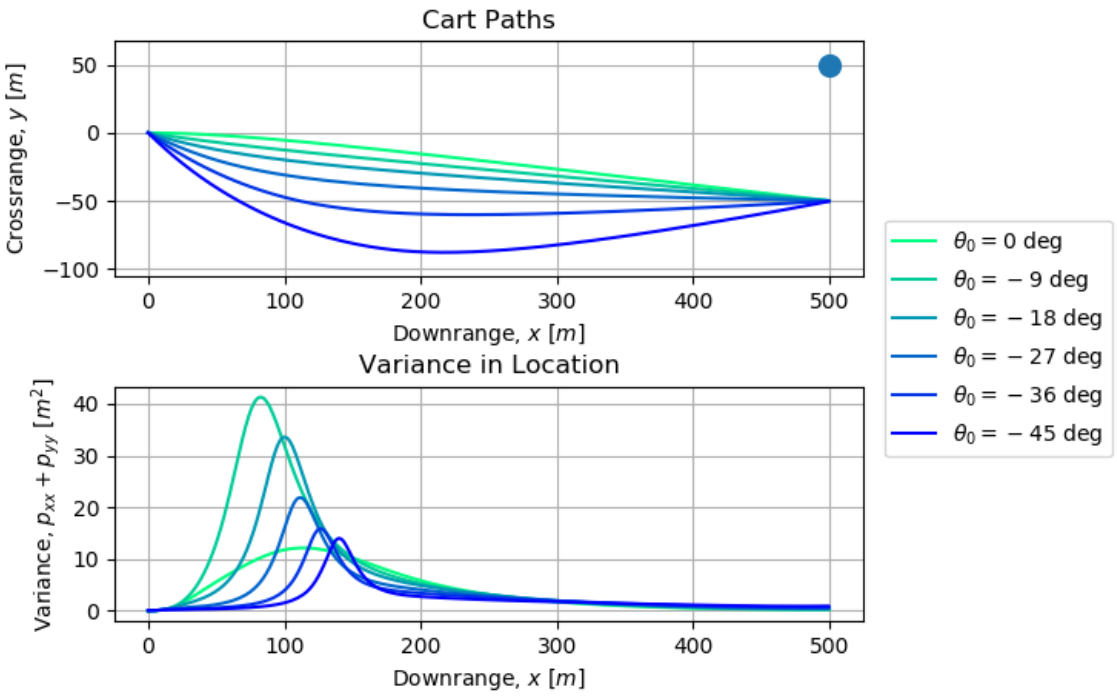

Figure 4.10. Radically Different Paths With Variances That Converge to the Same Value

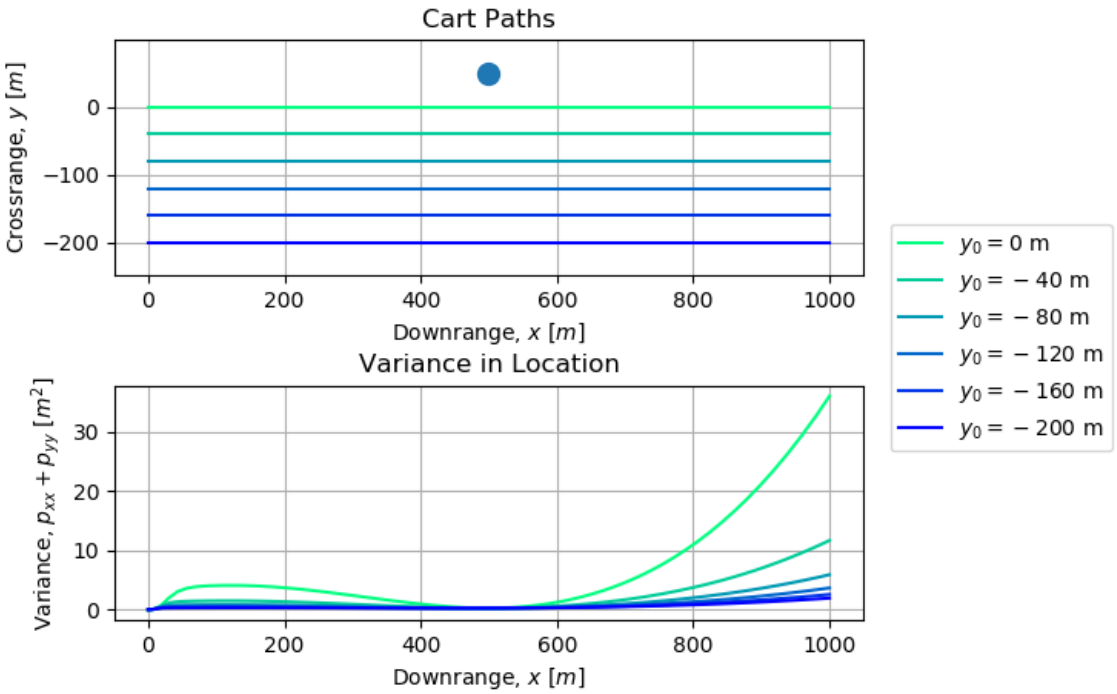

Figure 4.11. Convergence and Divergence of Variance as Vehicle Crosses Beacon

4.4 Aircraft Descent Problem

The methods described in this report can be applied to larger and more complex problems particularly in the aerospace field. This section demonstrates that with a projectile descent problem. The ability to perform trade studies is also demonstrated with this problem.

4.4.1 Problem Formulation

The descent problem below is diagrammed in Fig. 4.12. It consists of a supersonic projectile gliding to a target on the ground with minimum location estimation errors. The control is angle of attack rate, which is limited. Vehicle motion is confined to a 2-D vertical plane with altitude h and downrange s. The other two states are velocity v and flight path angle γ. Aerodynamic forces are calculated with a lift coefficient linear with respect to angle of attack, a drag coefficient parabolic with respect to the lift coefficient, and an exponential atmosphere meaning density decreases exponentially with increasing altitude. These dynamics are described in Eqs. (4.23) to (4.34) with constants modified from a projectile outlined in [22]. The vehicle measures its bearing from a point behind the initial location by Eq. (4.27). This may be thought of as the launch vehicle tracking the projectile and sending the information to it or other similar setup. Practically, the placement of that point was to avoid issues like those discussed above in Section 4.3.3.

$$\min J = p_{hh}(t_f) + p_{ss}(t_f) \tag{4.23}$$

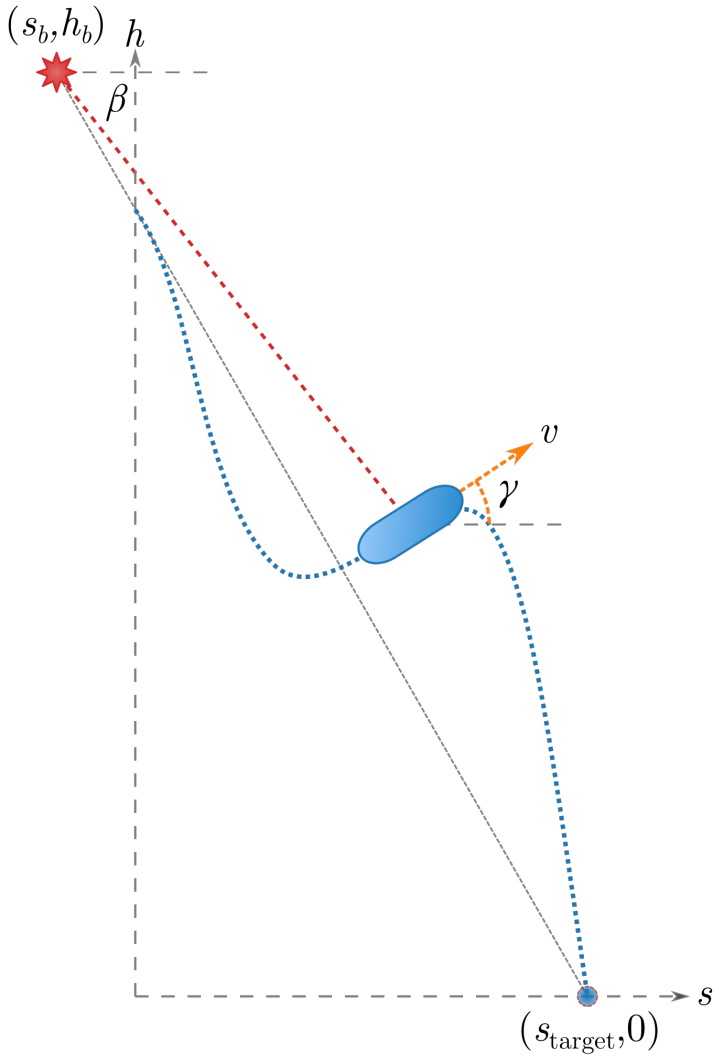

Figure 4.12. Diagram of Descent Problem

Subject to:

$$\boldsymbol{f} = \begin{bmatrix} \dot{h} \\ \dot{s} \\ \dot{v} \\ \dot{\gamma} \end{bmatrix} = \begin{bmatrix} v \sin\gamma \\ v \cos\gamma \\ -\frac{D}{m} - g \sin\gamma \\ \frac{L}{mv} - \frac{g}{v} \cos\gamma \end{bmatrix} \tag{4.24}$$

$$\Psi_0 = \begin{bmatrix} h(0) - h_0 \\ s(0) \\ v(0) - v_0 \\ \gamma(0) - \tan^{-1}\frac{h_0 - h_f}{s_f} \end{bmatrix} = \mathbf{0}, \qquad \Psi_f = \begin{bmatrix} h(t_f) - h_f \\ s(t_f) - s_f \\ v(t_f) - v_f \end{bmatrix} = \mathbf{0} \tag{4.25}$$

Where:

$$\begin{aligned} L &= \frac{1}{2}\rho v^2 C_L A_{\text{ref}}, & C_L &= C_{L,\alpha}\alpha \\ D &= \frac{1}{2}\rho v^2 C_D A_{\text{ref}}, & C_D &= C_{D,0} + \frac{C_L^2}{\pi e A_{\text{ref}}} \\ \rho &= \rho_0 e^{-\frac{h}{h_{\text{ref}}}} \end{aligned} \tag{4.26}$$

With measurement:

$$\boldsymbol{h} = \beta = \arctan 2(h_b - h, s_b - s) \tag{4.27}$$

With covariance dynamics:

$$\dot{P} = FP + PF^T - PHR^{-1}HP + GQG^T \tag{4.28}$$

$$Q = \frac{E\left\{\boldsymbol{w}(t)\boldsymbol{w}^T(\tau)\right\}}{\delta\left(t-\tau\right)} = \begin{bmatrix} \sigma_{\dot{v}}^2 & 0 \\ 0 & \sigma_{\dot{\gamma}}^2 \end{bmatrix} \tag{4.29}$$

$$R = \frac{E\left\{\boldsymbol{v}(t)\boldsymbol{v}^T(\tau)\right\}}{\delta\left(t-\tau\right)} = \begin{bmatrix} \sigma_\beta^2 \end{bmatrix} \tag{4.30}$$

$$F = \begin{bmatrix} 0 & 0 & \sin\gamma & v\cos\gamma \\ 0 & 0 & \cos\gamma & -v\sin\gamma \\ \frac{A_{ref}C_D v^2\rho}{2mh_{\text{ref}}} & 0 & -\frac{A_{\text{ref}}vC_D\rho}{m} & -g\cos\gamma \\ -\frac{0.5A_{\text{ref}}C_L v\rho}{mh_{\text{ref}}} & 0 & \frac{0.5A_{\text{ref}}C_L\rho}{m} & \frac{g\sin\gamma}{v} \end{bmatrix} \tag{4.31}$$

$$H = \frac{\partial \boldsymbol{h}}{\partial \boldsymbol{x}} = \begin{bmatrix} \frac{(s-s_{\text{target}})}{h^2+(s-s_{\text{target}})^2} & -\frac{h}{h^2+(s-s_{\text{target}})^2} & 0 & 1 \end{bmatrix} \tag{4.32}$$

$$G = \begin{bmatrix} 0 & 0 \\ 0 & 0 \\ 1 & 0 \\ 0 & 1 \end{bmatrix} \tag{4.33}$$

With parameters:

$$\begin{aligned} C_{L,\alpha} &= 0.48\,\text{deg}^{-1} & C_{D,0} &= 0.5 & m &= 50\,\text{kg} \\ AR &= 4.5 & e_0 &= 0.7 & A_{\text{ref}} &= 0.0127\,\text{m}^2 \\ \rho_0 &= 1.225\,\text{kg/m}^3 & h_{\text{ref}} &= 9500\,\text{m} & g &= 9.81\,\text{m/s}^2 \\ \sigma_{\dot{v}} &= 0.1\,\text{m/s}^{\frac{3}{2}} & \sigma_{\dot{\gamma}} &= 0.05\,\text{deg}/\sqrt{\text{s}} & \sigma_\beta &= 0.1\,\text{deg}\sqrt{\text{s}} \\ v_0 &= 900\,\text{m/s} & h_0 &= 10000\,\text{m} & s_{\text{target}} &= 1000\,\text{m} \end{aligned} \tag{4.34}$$

4.4.2 Results

The results for this problem are in Fig. 4.13 compared with the trajectory that maximizes terminal velocity. By performing the s-curve, like those discussed in [2], the vehicle is able to achieve 28.6% reduction in the variance, from 67.7 m^2 to 48.3 m^2, in the terminal location. Like the single cart problem, one variance term dominates

the total. In this case, p_{ss} is about an order of magnitude larger. This results in the total variance being minimized despite p_{hh} being larger than the maximum velocity case. The reduction in state estimation errors comes at the cost of terminal velocity. For that reason, the terminal velocity was fixed to 350 m/s so that the vehicle would not slow too much. The terminal velocity constraint also reduces the control effort exerted. Despite the control constraint not being active, solving the problem using the constraint directly exhibits numerical issues from it as explained in Section 3.4.2. Still the absence of features like those in the cart problem, such as large regions that do not affect the objective and absence of forcing term, make the aircraft descent problem more numerically stable.

Including the control path cost $L = k_{en}u^2$ (Section 3.4.3) results in a problem that is generally easier for the designer to solve while still obtaining satisfactory results. The optimized trajectories with the path cost are presented in Fig. 4.14 for several values of k_{en}. The minimum terminal location variance of these trajectories is 48.7 m^2, a 28.0% reduction in variance. There is thus a penalty for the numerically more stable method, but the difference is only 0.83% of the optimal value. This is surprising because the trajectories differ significantly. The control constraint version approaches the target from a shallower angle than the maximum velocity case. On the other hand, the control cost case, flies over the target then turns to hit it. The great difference, but similar objective values point towards the existence of multiple local optima.

Varying the value of k_{en} indicates the bounded nature of the objective function. As k_{en} is made smaller, diminishing reductions in variance are seen as in the lower left plot of Fig. 4.14. Still, the maximum angle of attack achieved increases quadratically with decreasing $\log_{10} k_{en}$. A designer therefore can balance the terminal variance with the amount of control that is used.

By making the problem numerically more stable, trade studies may be performed on the trajectory vehicle parameters. In order to demonstrate this, Fig. 4.15 solves the problem for several terminal velocities. As the terminal velocity increases, the

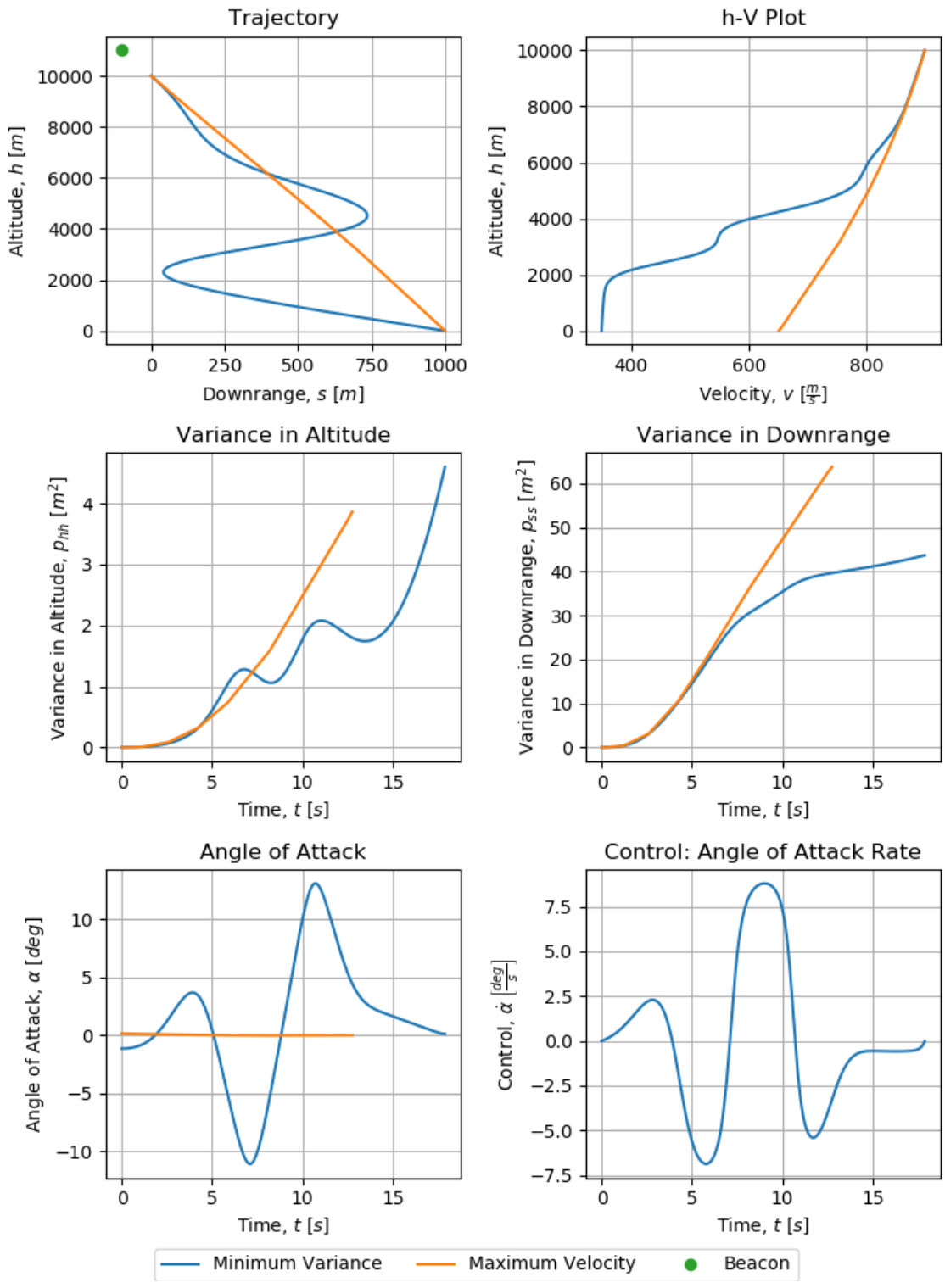

Figure 4.13. Results from Descent Problem Using Control Constraints

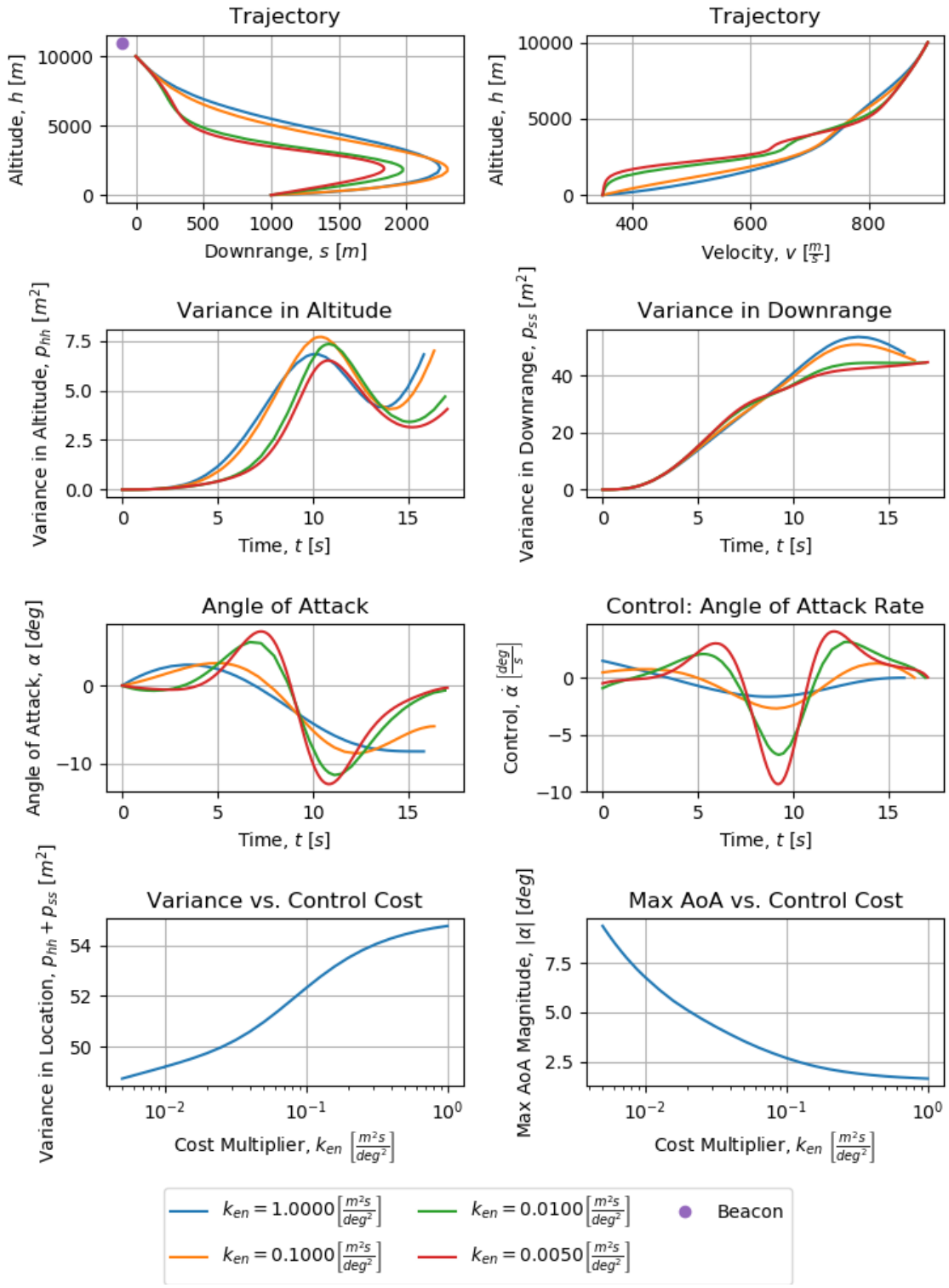

Figure 4.14. Results from Descent Problem Using Control Energy Cost

shape of the control profile does not change substantially, but instead decreases in magnitude. The variance in the downrange s is more affected by terminal velocity than variance in altitude. Minimal terminal variance in location is roughly linear with terminal velocity presenting another trajectory design choice. The same type of trade may be performed on the target location. This is shown in Fig. 4.16. As downrange increases, so does the variance. While changing the target position, the variance in altitude is more greatly affected for this range. The magnitude of the control exerted does not change much with downrange. Instead, the difference in variance is likely attributable to the final location relative to the beacon.

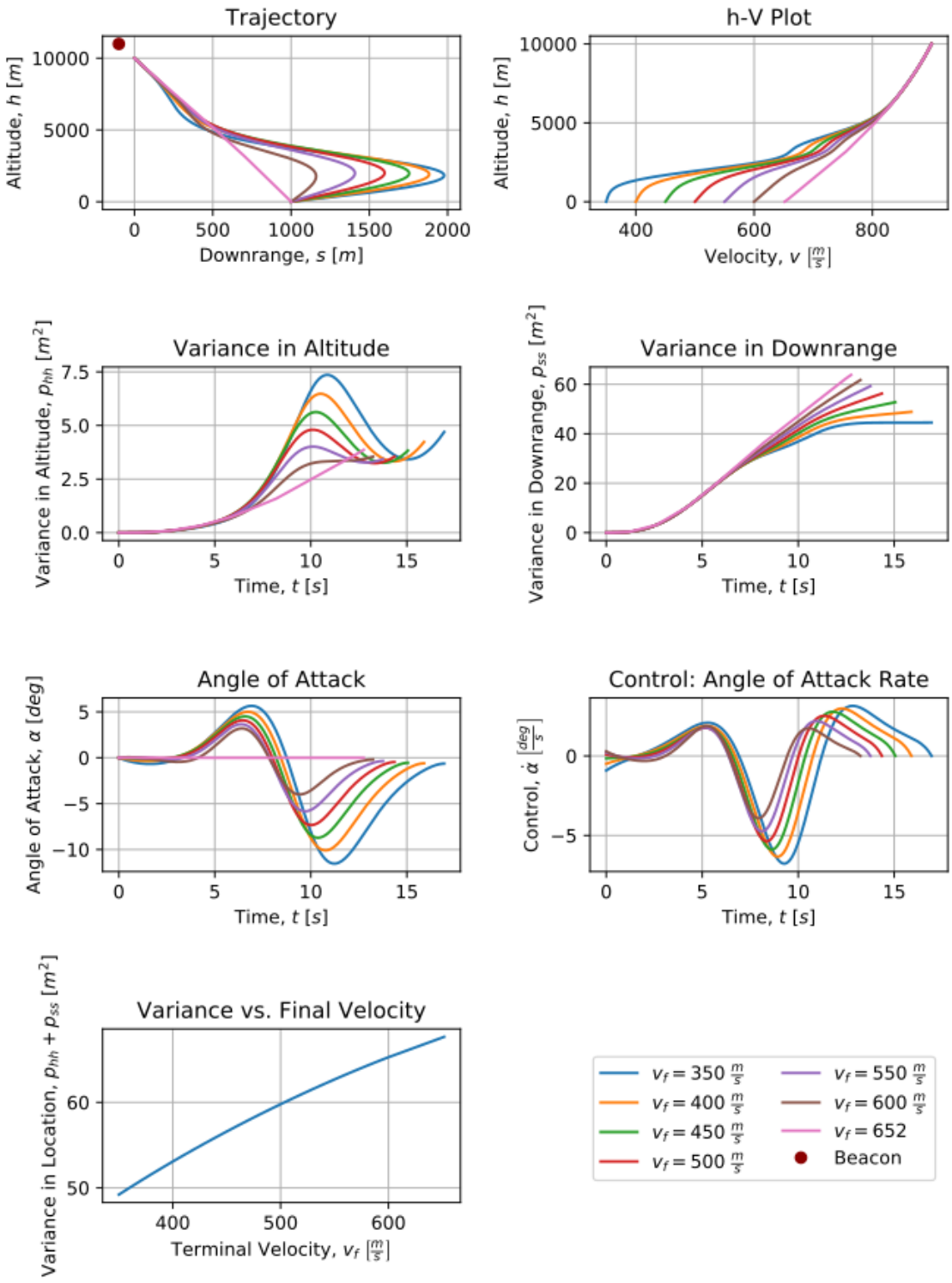

Figure 4.15. Variation of Optimal Trajectory With Changes in Terminal Velocity Constraint

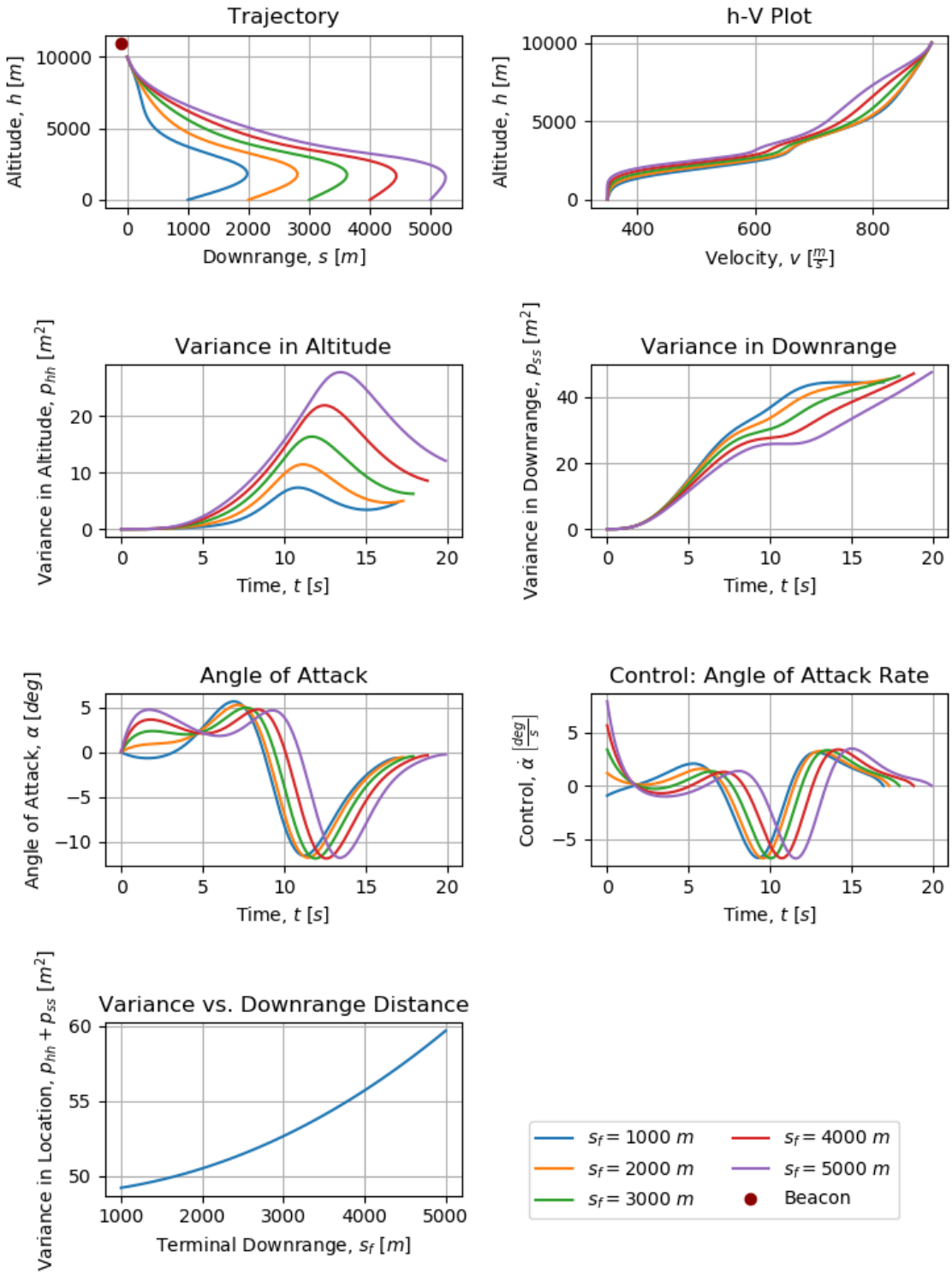

Figure 4.16. Variation of Optimal Trajectory With Changes in Target Location

5. SUMMARY

This study successfully implemented indirect optimization methods to problems that seek to minimize state estimation errors. The state estimation errors are approximated by use of extended Kalman filters. The equations for the covariance matrix may be propagated along side the original equations of motion and used in the objectives in an optimal control problem. Optimal control theory, an indirect method, is the chosen method to solve the problem in order to produce high quality optimal trajectories.

There are several special considerations that need to be address to solve navigation based optimization problems. The first is the large size of many of these problems. Because the number of additional covariance grows by $\frac{n(n+1)}{2}$ where n is the number of states, a problem's size can easily be computationally prohibitive. Additional numerical problems may arise particularly from the difference in size between a vehicle's states and those states' standard deviations. This is addressed particularly with different scaling techniques. Moreover, applying optimal control theory is complicated by the length of the dynamic equations of the states and costates. This is avoided by using a linear control with a specially applied control constraint or control energy path cost.

Despite not being able to solve the dual cart cart problem originally posed by Rutkowski et. al [5], the methods were successfully applied to a simpler single cart variation and an aircraft descent problem. An additional 1-D train problem is useful to show possible difficulties with solving these navigation-based problems, mainly the tendency of control extremes and possible existence of regions that do not affect the objective. By using trajectory optimization, a 96% reduction in terminal location estimation variance, from 4.72 m^2 to 0.184 m^2, was achieved with the single cart

problem. This example also further illuminates these problems first by highlighting the role of the dependency of the measurement on the states of interest.

Another necessary consideration is the possible existence of regions of the trajectory that do not affect the objective. The final problem type examined is a projectile descent example. Terminal location variance decreased by 28.6% by following the optimal path demonstrating the applicability of these methods to aerospace problems. The problem also can exhibit the utility of a control energy cost instead of control constraints. Using control energy cost made the problem numerically easier to solve with only a 0.83% deviation from the optimal value. Ultimately, this implies that it may be easier to solve multi-objective formulations because they make the problem more sensitive to the path when the minimum variance is bounded.

Future work should include expanding these methods to larger and more complicated problems such as the full dual cart one. To be able to do this, the lessons demonstrated here must be applied, especially the awareness of insensitivities of variance to certain sections of the paths. Additional work has to address the increasing size of problem, because this appears to be the limiting factor to applying these generally.

REFERENCES

[1] D. R. Vander Stoep. Trajectory Shaping for the Minimization of State-Variable Estimation Errors. *Transactions on Automatic Control*, AC-13(3):284–286, June 1968.

[2] Mitch Bryson and Salah Sukkarieh. Observability analysis and active control for airborne SLAM. *IEEE Transactions on Aerospace and Electronic Systems*, 44(1), 2008.

[3] Laurie N. Bose and Arthur G. Richards. Determining Accurate visual Slam Trajectories Using Sequential Monte Carlo Optimization. American Institute of Aeronautics and Astronautics, August 2013.

[4] Adam Rutkowski. The most accurate path from point A to point B is not necessarily a straight line. In *AIAA Guidance, Navigation, and Control Conference*, page 4761, 2012.

[5] Adam J. Rutkowski, Brian K. Taylor, Martin J. Eilders, Kevin M. Brink, and Clark N. Taylor. Path Planning for Cooperative Navigation with Inter-Agent Measurements. In *ION 2015 Pacific PNT Meeting*, pages 344–349, Honolulu, Hawaii, April 2015. Institute of Navigation.

[6] Adam J Rutkowski, Jamie E Barnes, and Andrew T Smith. Path planning for optimal cooperative navigation. pages 359–365. IEEE, April 2016.

[7] Yoko Watanabe, Eric Johnson, and Anthony Calise. Stochastically optimized monocular vision-based guidance design. In *AIAA Guidance, Navigation and Control Conference and Exhibit*, page 6865, 2007.

[8] Todd V. Small. *Optimal Trajectory-Shaping with Sensitivity and Covariance Technique*. PhD thesis, Massachusetts Institute of Technology, Cambridge, MA, May 2010.

[9] Thomas Antony. Rapid indirect trajectory optimization on highly parallel computing architectures. Master's thesis, Purdue University, 2014.

[10] James M. Longuski. *Optimal control with aerospace applications*. Springer, New York, 2013.

[11] John T. Betts. Survey of Numerical Methods for Trajectory Optimization. *Journal of Guidance, Control, and Dynamics*, 21(2):193–207, March 1998.

[12] Michael J. Grant and Robert D. Braun. Rapid Indirect Trajectory Optimization for Conceptual Design of Hypersonic Missions. *Journal of Spacecraft and Rockets*, 52(1):177–182, January 2015.

[13] Kshitij Mall and Michael James Grant. Epsilon-Trig Regularization Method for Bang-Bang Optimal Control Problems. *Journal of Optimization Theory and Applications*, 174(2):500–517, August 2017.

[14] Divya Garg, William W. Hager, and Anil V. Rao. Pseudospectral methods for solving infinite-horizon optimal control problems. *Automatica*, 47(4):829–837, April 2011.

[15] Harish Saranathan. *Algorithmic Advances to Increase the Fidelity of Conceptual Hypersonic Mission Design*. Ph.D., Purdue University, Ann Arbor, 2018. 10792495.

[16] Arthur E. Bryson and Yu-Chi Ho. *Applied optimal control: optimization, estimation, and control*. Hemisphere Pub. Corp. ; distributed by Halsted Press, Washington : New York, rev. printing edition, 1975.

[17] John L. Crassidis and John L. Junkins. *Optimal estimation of dynamic systems*. Number 24 in Chapman & Hall/CRC applied mathematics & nonlinear science. CRC Press, Boca Raton, FL, 2nd ed edition, 2012.

[18] Simon J Julier Je and K Uhlmann. A New Extension of the Kalman Filter to Nonlinear Systems. page 12.

[19] Michael J. Sparapany. Towards the real-time application of indirect methods for hypersonic missions. Master's thesis, Purdue University, 2015.

[20] Vivek Vittaldev, Ryan P. Russell, Nitin Arora, and David Gaylor. Second-order Kalman filters using multi-complex step derivatives. In *Proceedings of the AAS/AIAA Space Flight Mechanics Meeting, Kauai, Hawaii*, 2012.

[21] Thomas Antony and Michael J. Grant. Path Constraint Regularization in Optimal Control Problems using Saturation Functions. American Institute of Aeronautics and Astronautics, January 2018.

[22] Nichols, J. O. Analysis and compilation of missile aerodynamic data. Volume 1: Data presentation and analysis. Technical Report 19770021140, Auburn University; NASA, Alabama, United States, May 1977.